Modeling Approach to Transient Behaviors in Miscible Fluids with Two Layers

Toshio Ishikawa

Research Institute for Mathematical Sciences,
Kyoto University, Kyoto, Japan

December, 2022

Abstract

Many methods have been exploited to explain the mechanism of structure formation in flows, including the linear stability analysis, the bifurcation theory, and the explanation as a dynamical system. These standard approaches assume that the system has a steady or time-periodic solution. If the system under analysis does not have such a solution, one has to develop a different method. To propose some solution to this problem, we treat a miscible two-layer thermal convection system as an example.

We performed a numerical simulation of the system and observed two types of convection patterns; one is viscous coupling, and the other is thermal coupling. The viscous coupling pattern arises initially, while a thermal coupling pattern does after a certain time. This transient feature should be originated from the evolution of the transitional layer between two miscible fluids, which becomes thicker and unclear as time goes on due to the continuous diffusion of the concentration. In this system, therefore, we have no steady or time-periodic state, and it is not straightforward to employ the standard stability analyses, which often assume the existence of a steady or time-periodic state. It is in contrast to the case of immiscible fluids, where there remains a definite interface between the two fluids throughout time development, so the standard approaches are available because the system has a steady state.

To cope with this problem, we introduce a model in which the width of the transitional layer between the upper and lower layers (δ) is kept constant in the horizontal average. The standard approaches can be applied to this model because it has a steady state with two-layer structure. Both the linear stability of a stationary state of the model and nonlinear time-periodic solutions implies that viscous coupling is preferred when the width of the transitional layer δ is small, and thermal coupling is preferred when δ is large. Furthermore the transition from viscous coupling to thermal coupling is observed at $\delta \approx 0.02$ in all cases. These results are consistent with our numerical integration of the original system because the width of the transitional layer is observed to extend as time develops. We can also interpret the results as consistent with previous studies on convection systems of immiscible fluids by considering that their analyses were for infinitesimal transitional layer.

Our modeling approach presents a way to explain transient behavior of flow patterns observed in the two-layer convection system. We discuss what might be the key features of transient phenomena that enable similar approaches to explain their mechanism.

Contents

1 Introduction **7**
- 1.1 Standard theoretical approaches to structure formation 7
- 1.2 Structure formation in two-layer thermal convection system . . . 8
- 1.3 The approach we propose in this thesis 12

2 Numerical Experiments of Convection in Two Miscible Layers **13**
- 2.1 Governing equations and boundary and initial conditions 13
- 2.2 Experimental setup 15
- 2.3 Results of numerical experiments 16

3 Model Analysis of the Convection of the Miscible Fluids **21**
- 3.1 Model with a fixed transitional layer 21
- 3.2 Linear stability problem of the stationary state 22
- 3.3 Neutral modes 23
- 3.4 Unstable modes at $Ra = 3200$ 26
- 3.5 Asymptotic behavior of nonlinear states after a long time integration 28
- 3.6 Projections to viscous coupling and thermal coupling function spaces 32
- 3.7 Time integration of viscous coupling and thermal coupling convections 33

4 Discussions and Conclusions **37**
- 4.1 Modeling convection system with two miscible layers 37
- 4.2 Modeling approach to transient phenomena in general 39

A Proofs of Some Claims **41**
- A.1 Invariance of symmetry of the model system in time development 41
- A.2 Orthogonality of thermal and viscous coupling functional spaces 42

References **49**

Chapter 1

Introduction

One of the central concerns in fluid physics is the elucidation of the formation mechanisms of flow patterns. We humans living on the Earth are surrounded by many fluids, including air and water. They often show characteristic structures, such as cloud patterns, whirlpools, and convection currents in pots. In addition to what we see in our daily lives, we can also see the layered temperature distribution in the oceans, convective structures inside the Earth, and vortices on Jupiter. It is natural in physics to try to explain how these various structures appear in fluid phenomena. In particular, many theoretical physicists have explained the mechanism behind the pattern formation by analyzing behaviors of solutions of basic equations such as Navier-Stokes equations and those derived from them.

1.1 Standard theoretical approaches to structure formation

The most basic and widely used method is linear stability analysis. In this method, it is discussed whether the stationary solution of a system is stable or unstable against infinitesimal disturbances. The case in which the amplitude decays exponentially for any infinitesimal disturbances is called linearly stable. In contrast, the case in which the amplitude grows for a specific infinitesimal disturbance is called linearly unstable. The equation of disturbance is linear because the terms with or higher than the second order are neglected in the derivation process. For this reason, this method is called "linear" stability analysis. The most successful example of this method is the Rayleigh-Bénard convection system. This fluid system has a temperature difference at the upper and lower boundaries. The stationary solution of this system is linearly stable when the Rayleigh number (the nondimensionalized temperature difference between the upper and lower boundaries) is smaller than a particular critical value and becomes linearly unstable when it exceeds that value. The convection structure observed in experiments corresponds well to that of the critical mode,

the disturbance that becomes unstable at the critical value. The linear stability provides one explanation for the mechanism of convection onset.

Several methods have been developed that consider the nonlinearity of fluid equations. The bifurcation analysis is a theory that continuously traces the process by which a steady or time-periodic solution becomes unstable, and a new solution emerges. For example, in the Rayleigh-Bénard system, the steady convective solution realized when the Rayleigh number is slightly higher than the critical value continuously "connects" to the quiescent state when the Rayleigh number is gradually decreased. In the opposite view, when the Rayleigh number is gradually increased from the region lower than the critical value, the stationary solution "bifurcates" into two solutions, itself and convection. By varying Rayleigh and Prandtl numbers, one observes similar bifurcations, e.g., a time-periodic solution bifurcates from stationary convection.

There are methods to explain the nonlinear dynamics of fluids in terms of dynamical systems, especially time-periodic orbits. The structure formation in sustaining turbulence is often discussed using this method. Typical time-periodic solutions embedded in turbulent flows have saddle-like structures, i.e., in the functional space, they attract in some directions and repel in others. The actual flow realized in experiments is not necessarily a time-periodic solution, but the flow changes as it moves around between time-periodic solutions embedded nearby because of the saddle-like structure of those time-periodic solutions. The periodic solutions are, so to speak, "skeletons" of the flow. For example, it has been reported that the characteristic structure and behavior of a sustained turbulent flow appear in the time-periodic solution of the system [10].

1.2 Structure formation in two-layer thermal convection system

The methods described in the previous section are powerful and effective in many cases, but they are not universal. In particular, all methods require stationary or time-periodic solutions to the system. Therefore, if such a solution does not exist in the system under analysis, it is necessary to devise another method. This thesis aims to propose a practical approach to the problem of structure formation in systems without stationary or periodic solutions. We take a two-layer thermal convection system with no stationary state (with a two-layered structure) and introduce an analytical method to explain the transition mechanism of those patterns.

The two-layer thermal convection system we deal with is one in which two fluid layers overlap vertically. Gravity acts downward, and the upper and lower boundary surfaces are kept at constant temperatures, with the lower surface being hotter than the upper. It is a generalization of the Rayleigh-Bénard system, a single-layer convection system. Since fluid systems in the real world do not necessarily consist of fluids with uniform properties, thermal convection systems consisting of two or more layers are good models of phenomena in various

fields. For example, a two-layer convection system is a model of fluid layers of different salinities that form in the ocean. Also, the convective structure of the Earth's mantle is discussed using a two-layer convection system. Two-layer and multi-layer convection systems are also used in engineering applications to model plasmas in fusion reactors[24] and molten materials[15].

When investigating a two-layer convection system, the treatment differs depending on whether the two fluids are miscible or immiscible. Immiscibility is the nature of two fluids that do not mix, for instance, water and oil. The system has a clear boundary between the two fluids. Therefore there is a stationary solution where the two fluids exist across the interface. In contrast, miscibility is the nature of two fluids that mix by diffusion effects, for instance, saline and fresh water. The boundary of two-fluid gradually becomes blurred by diffusion. Thus the system has a transitional layer with continuously changing properties, not a definite interface. The state in which two layers exist is not steady because such a state gradually approaches to single-layer state.

In this thesis, we treat a two-layer thermal convection problem with two miscible fluids. Specifically, we treat the system with the following features:

- Two-dimensional system with upper and lower layers, each consisting of solutions of the same type of solute at different concentrations.

- At the initial time, both layers have constant concentrations, where the lower one is heavier. The temperature field is assumed to be the heat conduction solution, i.e., a linear temperature distribution in the vertical direction.

- Time evolution of the concentration field is governed by the advection-diffusion equation. A well-defined interface exists only at the initial time, after which there is only a transitional layer between the two fluids with continuously changing concentration.

More detailed descriptions will be given at Sections 2.1 and 2.2.

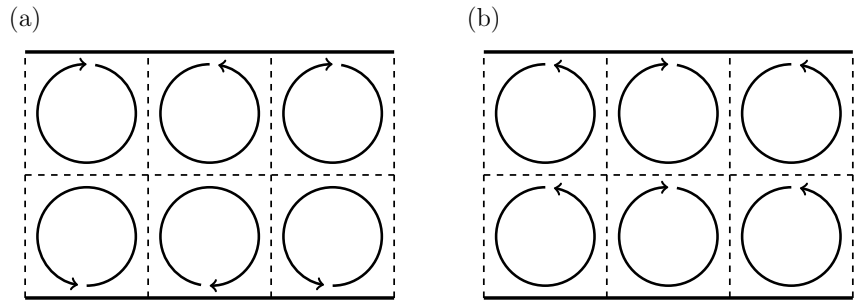

Figure 1.1: Sketch of two typical patterns of convection in two-layer system: (a) viscous coupling and (b) thermal coupling.

We observed two types of convection patterns through numerical integration (Chapter 2) for specific parameters, viscous and thermal coupling, shown in Figure 1.1. In viscous coupling, the convection in the upper layer rotates opposite to that just below it. In contrast, in thermal coupling, the convection in the upper layer rotates in the same direction as just below it. In our numerical integration, we observed a viscous coupling pattern in the initial stage and a thermal coupling pattern after a certain time. Study of this transition phenomenon is the main objective of this thesis. In Section 2.3, we will describe the behaviors in more detail.

Viscous and thermal coupling patterns have been investigated in studies of immiscible two-layer thermal convection systems. Rasenat *et al.* (1989) [16] performed laboratory experiments and linear stability analysis over a wide range of parameters to investigate which convection structures are preferred. The characteristics of the system they analyzed are as follows:

- The system consists of two fluids, an upper and a lower layer separated by an interface, with gravity acting downward.
- The upper and lower boundary surfaces are kept at constant temperatures, with the lower surface set to be hotter.
- In addition to the temperatures of the top and bottom surfaces, the system has a lot of control parameters: the physical properties of the fluid in each layer, the width of each layer, the gradient of the temperature field in each layer, and the surface tension of the interface and thermal conductivity.
- At the interface, kinematic boundary conditions are assigned, such that there is no material penetration through the interface.

This system has a stationary solution where the interface is horizontal and steady. The authors performed its linear stability analysis and found the following unstable modes:

- Steady viscous coupling mode
- Steady thermal coupling mode
- Time-dependent mode, oscillating between viscous coupling and thermal coupling

In particular, the neutral mode they found was viscous coupling mode under equal widths of the upper and lower fluid layers and the same physical properties other than density. Davanille *et al.* (2002) [5] performed a linear stability analysis in the same manner as Rasenat *et al.* in the high Prandtl number limits and laboratory experiments to verify the results. They investigated how the instability of the interface changes with Buoyancy number B, the ratio of the material density difference between the upper and lower layers to the density change due to the temperature difference between the upper and lower boundaries. Although they are mainly interested in the instability at the interface,

they also investigated the convective structure in the layers and reported that a stratified regime (corresponding to viscous coupling in this thesis) is selected when the widths of the two layers are equal. Note that the word "miscible" in the title of their paper means that they assumed no surface tension at the interface. Their linear stability analysis was based on the assumption that the effect of material diffusion near the interface was negligible. Nepomnyanscy [14] also investigated the convective structure of the two-layer system. They studied the conditions under which the most unstable mode is oscillatory, considering thermocapillary effects and interfacial heat release.

On the other hand, publications of viscous and thermal coupling in miscible two-layer fluids are somewhat limited in number. The report by Yanagisawa and Kurita [25] is one of a few that investigated this phenomenon through laboratory experiments. According to their report, the convection pattern evolved as follows:

- Initially, the structure of thermal coupling was realized.
- After some time, it changed to viscous coupling.
- After thermal coupling was observed again for a short time, the interface was destabilized, and the whole system was mixed.

They discussed the transition of the patterns using the width of the transitional layer formed by material diffusion. Specifically, they discussed that thermal coupling was selected in the early stage when the transition layer width was thick because the temperature distribution was a more important factor in determining the structure than horizontal shear, and viscous coupling was selected in the middle stage when the transition layer width became thinner because the horizontal shear became more dominant. They presented an idea to understand the transition of the patterns but did not provide any theoretical or quantitative analysis to verify this idea. If their argument is correct, the width of the transition layer, which is a quantity coming from miscibility, plays an essential role in selecting the coupling pattern. It means that physical phenomena are occurring that cannot be captured by the analysis based on the assumption of an infinitesimal interface, as described in the previous paragraph.

The only steady state of a miscible two-layer thermal convection system is the well-mixed single-layer state that realizes after a sufficiently long time. The analysis using a steady state with linearly varying temperature and concentration fields has been classically well performed. The structures called "finger-salt" and "diffusive convection" can be obtained depending on temperature and concentration profiles [22]. These analyses provide a good description of convection structures near the interface. However, the patterns of convection that occur throughout each of the two layers, such as viscous and thermal coupling structures, cannot be obtained. In other words, the standard approaches to the single-layer steady state are not appropriate to investigate the mechanism by which the coupling pattern is realized. Thus we need a new analytical method that is not based on a steady-state solution.

1.3 The approach we propose in this thesis

Considering the results of previous studies on immiscible two-layer thermal convection systems, it seems natural also in the case of miscible fluids to apply the standard approaches to steady-state solutions with a two-layered structure to explore the viscous and thermal coupling patterns. However, it is impossible because the miscible two-layer thermal convection system does not have such a steady solution. Suppose we can somehow "freeze" the ever-changing two-layer state and define a model in which the two-layer state is the steady-state solution (Ishikawa *et al.* (2022) [9]). In that case, we can apply standard approaches to that model to analyze the unstable structure at that moment. The method we propose in this thesis achieves exactly this goal by neglecting some of the nonlinear terms in the original system's basic equations so that the horizontal mean of the concentration field is fixed.

In Chapter 2, we will review two-layer thermal convection system and present numerical experiment of the original system to show transient behavior of its solution. In Chapter 3, we will introduce our modeling approach and describe the results. The derivation of the model will be given at Section 3.1. In this model, the width of the transitional layer is "frozen" in the sense of the horizontal mean, and the transient nature of "approaching a one-layer state as time passes" is lost, so a stationary solution can be obtained in which the two-layer state is maintained. We perform a linear stability analysis on this steady-state solution and discuss the relationship between the width of the transition layer and the structure of linear stability. The settings and results of the linear stability analysis will be described in Sections 3.2, 3.3, 3.4. We also numerically obtain nonlinear solutions corresponding to viscous and thermal coupling patterns and investigate the change of the state when the width of the transition layer is varied. The results are given in Sections 3.5, 3.6 and 3.7. The results of both analyses explain the transition from viscous coupling to thermal coupling observed in the numerical experiments of the original system. Discussions and conclusions of analyses will be given in Chapter 4.

Chapter 2

Numerical Experiments of Convection in Two Miscible Layers

2.1 Governing equations and boundary and initial conditions

We consider two-dimensional double diffusive thermal convection in two horizontal layers of miscible fluids which initially have the same depth, one lying on top of the other, under downward gravity (Fig. 2.1). We apply Boussinesq approximation to the system. The physical properties of the fluids, such as basic density, viscosity and thermal diffusivity, are assumed to be the same and constant. We take the x and z axes in the horizontal and vertical directions, respectively. Let $z = 0$ be the initial boundary between the two fluids, which are definitely separated at $t = 0$.

To non-dimensionalize the equations, we take the initial depth of each fluid layer h as the length scale, h^2/D_T as the time scale (where D_T is a thermal diffusion coefficient), the temperature difference between the top and bottom boundaries ΔT as the temperature scale, and the initial concentration difference between the upper and lower layers ΔS as the concentration scale. Then the non-dimensional equations are,

$$\partial_t \boldsymbol{u} + (\boldsymbol{u} \cdot \nabla)\boldsymbol{u} = -\nabla p + RaPr(T - BS)\boldsymbol{k} + Pr\nabla^2 \boldsymbol{u}, \tag{2.1}$$

$$\nabla \cdot \boldsymbol{u} = 0, \tag{2.2}$$

$$\partial_t T + (\boldsymbol{u} \cdot \nabla)T = \nabla^2 T,$$

$$\partial_t S + (\boldsymbol{u} \cdot \nabla)S = \frac{1}{Le}\nabla^2 S,$$

where $\boldsymbol{u} = (u_x, u_z)$, T, S and p are non-dimensionalized velocity, temperature,

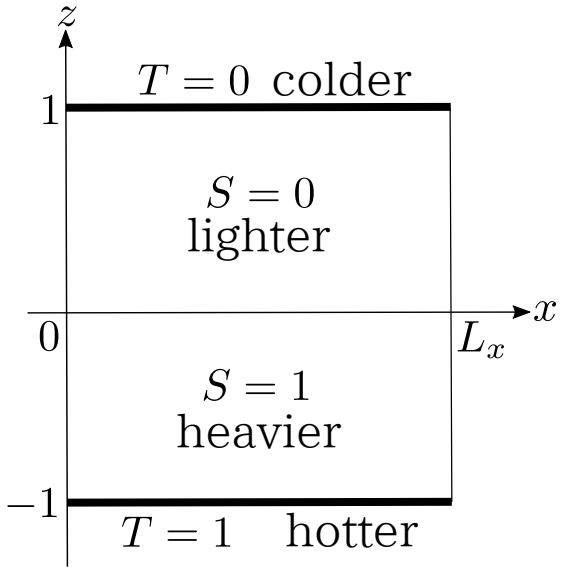

Figure 2.1: Initial configuration of a two-dimensional system of double diffusive thermal convection in two horizontal layers of miscible fluids under downward gravity. The fluid in the upper layer has lower concentration than the fluid in the lower layer. No concentration fluxes are assumed at the boundaries $z = \pm 1$, where the temperatures are held constant in a way that makes the bottom hotter than the top.

concentration and pressure, respectively, and $\boldsymbol{k}$ is the unit vector in the z direction. The operator ∇ is defined as (∂_x, ∂_z). The Rayleigh number Ra, the Prandtl number Pr, the buoyancy number B and the Lewis number Le in the equations are non-dimensional quantities defined by

$$Ra = \frac{\alpha_T g h^3 \Delta T}{D_T \nu}, \quad Pr = \frac{\nu}{D_T}, \quad B = \frac{\alpha_S \Delta S}{\alpha_T \Delta T}, \quad Le = \frac{D_T}{D_S},$$

where ν is the kinematic viscosity, g is gravitational acceleration, α_T and α_S are thermal and compositional expansion coefficients, respectively, and D_S is the compositional diffusion coefficient.

The horizontal boundary condition is periodic. The boundary conditions at the top and bottom boundaries are non-slip with fixed temperatures and null concentration fluxes as follows.

$$\boldsymbol{u}(x, \pm 1, t) = 0, \tag{2.3}$$

$$T(x, 1, t) = 0, \quad T(x, -1, t) = 1, \tag{2.4}$$

$$\partial_z S(x, 1, t) = 0, \quad \partial_z S(x, -1, t) = 0. \tag{2.5}$$

We introduce a stream function $\psi(x, z, t)$ that satisfies

$$u_x = \partial_z \psi, \quad u_z = -\partial_x \psi,$$

because of the incompressibility condition (2.2). By assuming no net horizontal flux and choosing a proper additive constant, we can rewrite the non-slip condition (2.3) as the boundary condition of the stream function at the top and bottom boundaries

$$\psi(x, \pm 1, t) = \partial_z \psi(x, \pm 1, t) = 0. \tag{2.6}$$

Taking the curl of (2.1) and rewriting non-linear terms using the Jacobian $J(a, b) = (\partial_z a)(\partial_x b) - (\partial_x a)(\partial_z b)$, we can deduce the evolution equations as

$$\partial_t \nabla^2 \psi + J(\psi, \nabla^2 \psi) = -RaPr\partial_x (T - BS) + Pr\nabla^2 \nabla^2 \psi, \tag{2.7}$$

$$\partial_t T + J(\psi, T) = \nabla^2 T, \tag{2.8}$$

$$\partial_t S + J(\psi, S) = \frac{1}{Le} \nabla^2 S. \tag{2.9}$$

2.2 Experimental setup

The vorticity-streamfunction method was used for solving the problem numerically. The stream function, temperature and concentration were spatially discretized by Fourier pseudo-spectral method in the x direction, and by finite difference method in the z direction. The horizontal system size was $L_x = 4\pi/2.6 \approx 4.83$ while the vertical size of each layer was 1. We set the equally spaced grid points as 192×101 in the x and z directions, respectively, and the truncation number 64 in the x direction, eliminating aliasing errors by the 1/3-rule. For the time stepping, we used the Crank-Nicolson scheme for linear terms, and the modified Euler scheme for nonlinear terms.

We explored a set of parameters that included the horizontal extent of the domain in which we can clearly observe the viscous coupling and thermal coupling patterns (Fig. 1.1) and the transition between these states. We chose the non-dimensional physical parameters as

$$Ra = 3200, \quad Pr = 10, \quad Le = 10^4, \quad B = 10. \tag{2.10}$$

The initial conditions for the temperature and concentration were

$$T(x, z, 0) = \frac{1}{2}(1 - z), \quad S(x, z, 0) = \begin{cases} 0 & (z > 0) \\ 1 & (z < 0) \end{cases}. \tag{2.11}$$

We took some non-zero initial conditions of ψ, one of which is in the following form:

$$\psi(x, z) = \left\{ \sin^2 \left[\frac{\pi(z-1)}{2} \right] + \sin^3 \left[\pi(z-1) \right] \right\} \exp \left\{ \sin \left(\frac{2\pi x}{L_x} \right) \right\}, \tag{2.12}$$

while the numerical results for other initial conditions did not affect our analysis described below.

2.3 Results of numerical experiments

Figure 2.2 shows the stream function ψ and the temperature deviation $\Theta \equiv T - T|_{t=0}$ in their early stage ($t = 0.7$). Here, we observe two streets of vortex arrays: the upper vortices rotate in the direction opposite to the lower vortices just below them (Fig. 2.2 (a)), and similarly the sign of the temperature deviation Θ is also opposite in the upper and lower vortices (Fig. 2.2 (b)). We call the state with this convection pattern viscous coupling.

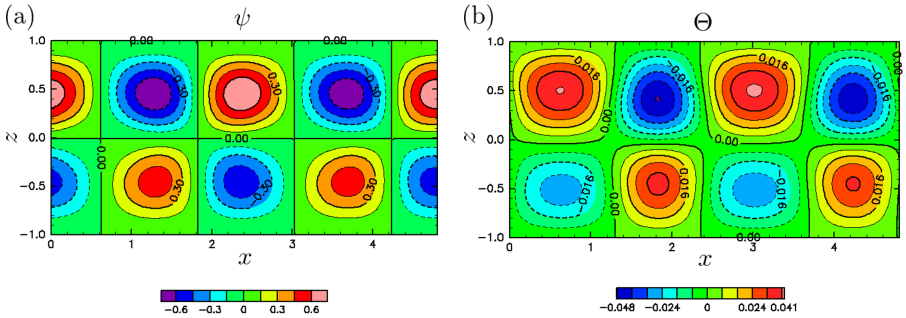

Figure 2.2: Snapshots of (a) the stream function ψ and (b) the temperature deviation Θ at $t = 0.70$. This convection pattern is identified as 'viscous coupling'.

During $1.0 \lesssim t \lesssim 2.3$, however, the viscous coupling pattern disappears and a different convection pattern appears as seen in Fig. 2.3, which shows the

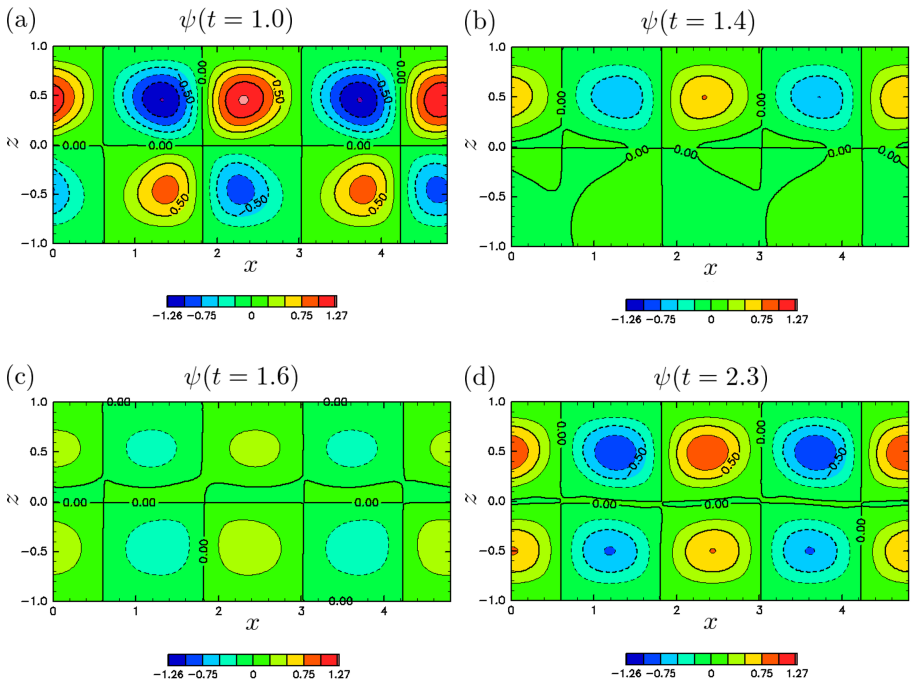

Figure 2.3: Snapshots of the stream function ψ at (a) $t = 1.0$, (b) 1.4, (c) 1.6 and (d) 2.3.

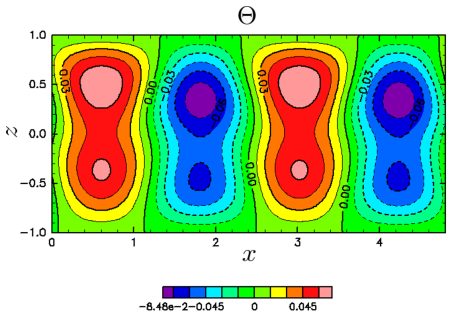

Figure 2.4: Temperature deviation Θ at $t = 2.3$. The sign is the same between the upper and lower layers.

stream function ψ during $1.0 \leq t \leq 2.3$. In the lower layer, the convection decays during $1.0 \lesssim t \lesssim 1.4$, and a new convection in the opposite direction grows during $1.4 \lesssim t \lesssim 2.3$, while the convection in the upper layer does not decay completely, and regrows for $1.6 \lesssim t \lesssim 2.3$. Then two streets of vortex array are formed at $t = 2.3$, in which the convection in the upper and lower layers rotates in the same direction. The sign of the temperature deviation Θ is also the same between the upper and lower vortices (Fig. 2.4). We call the state of this convection pattern thermal coupling.

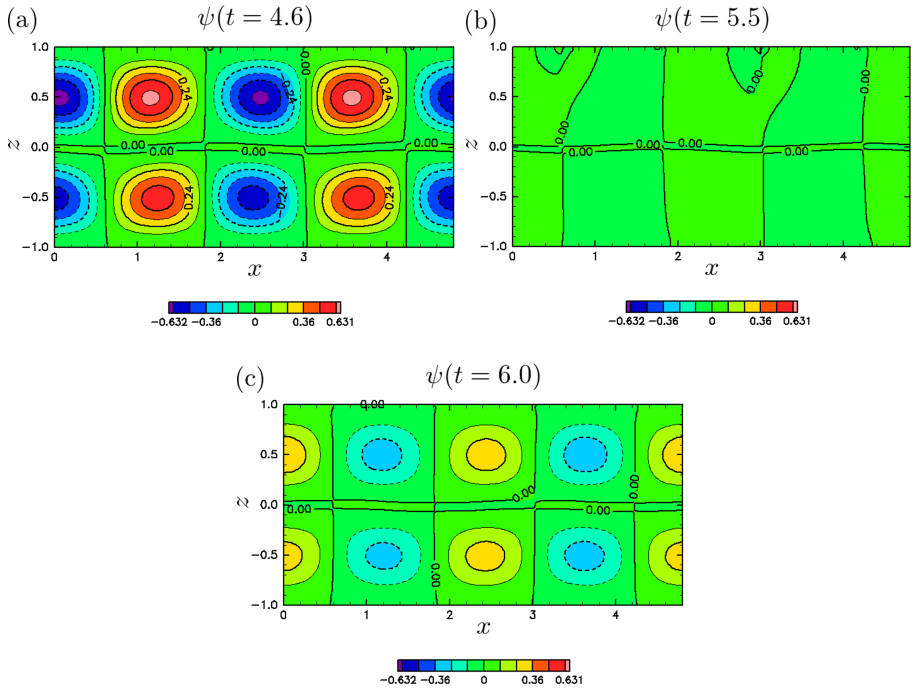

Figure 2.5: Snapshots of the stream function ψ at (a) $t = 4.6$, (b) 5.5 and (c) 6.0. The convection decays during $4.6 \lesssim t \lesssim 5.5$, and convection in the opposite direction grows during $5.5 \lesssim t \lesssim 6.0$.

The convection continues for some time, gradually decreasing in amplitude, and finally almost stops. Then the convection rotating in the opposite direction grows. This process takes place in parallel in both layers. This periodic oscillation continues but is gradually damped, and after a long time integration, the convection finally loses its clear pattern. The remnants of thermal coupling are observed at $t = 15.0$ (Fig. 2.6), but the amplitude of the convection is lower than that at $t = 2.3$ by two order of magnitude.

It can be seen from Fig. 2.2 (a), Fig. 2.3 (d), Fig. 2.5 (c) and Fig. 2.6 that, as time develops, the vertical scales of the convection vortices gradually decreases and the convection cells in the upper and lower layers become separated. This causes a decrease of the effective Rayleigh number for the convection and a

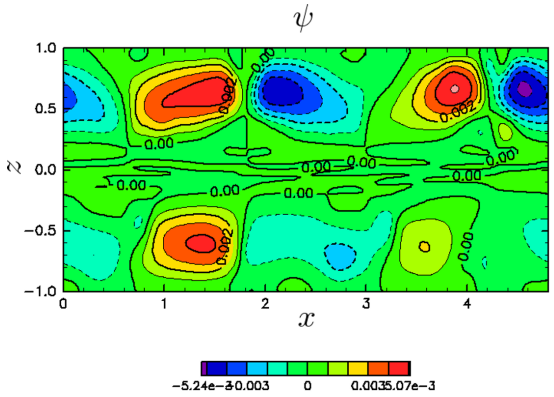

Figure 2.6: Stream function ψ at $t = 15.0$. The remnants of thermal coupling are observed. The amplitude of the convection is lower than that at $t = 2.3$ (Fig. 2.3 (d)) by two order of magnitude.

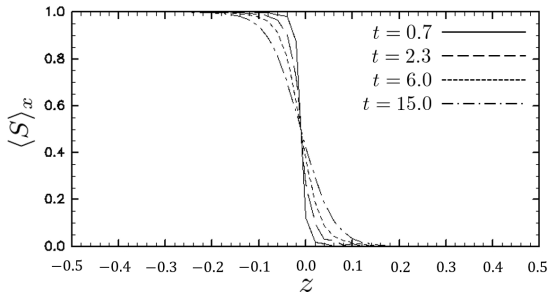

Figure 2.7: Horizontally averaged concentration $\langle S \rangle_x$ at $t = 0.7, 2.3, 6.0$ and 15.0 and $z = -0.5$ to 0.5. The horizontal average of the transitional layer gradually increases with time.

decline of its amplitude. The horizontal averages of the concentration field $\langle S \rangle_x$ at $t = 0.7, 2.3, 6.0$ and 15.0 are shown in Fig. 2.7, where $\langle \cdot \rangle_x$ stands for the horizontal average. The figure shows that the horizontal average of the transitional layer of the concentration is not steady, but gradually expands. For this reason, it is difficult to apply the standard techniques of dynamical systems such as linear stability analysis of equilibrium points or periodic orbits.

Chapter 3

Model Analysis of the Convection of the Miscible Fluids

3.1 Model with a fixed transitional layer

Because the transitional layer of miscible fluids continues to expand, the phenomena are transient through the time development. To apply standard procedures based on stationary states, we introduce an artificial model whose transitional layer has a constant width in the horizontal average through modification of the evolution equation of the concentration.

We decompose S into two parts:

$$S(x,z,t) = S_\delta(z) + \Sigma(x,z,t), \tag{3.1}$$

where

$$S_\delta(z) \equiv \frac{1}{2}\,\mathrm{erfc}\left(\frac{z}{\delta}\right), \quad \delta \equiv 2\sqrt{Le^{-1}t}, \quad \mathrm{erfc}(x) = \frac{2}{\sqrt{\pi}}\int_x^\infty e^{-\xi^2}d\xi$$

where S_δ corresponds to the time development of S when $\psi = 0$.

Here we devise a model system of equations to understand the transient behavior of the thermal convection of miscible fluids. A theoretical difficulty comes from the non-stationary nature of the transient behavior where the width of the transient layer becomes larger over the course of time development. Therefore we propose a model system in which the width of the horizontally averaged transient layer is kept constant.

For this purpose, a simple way may be to assume $S = S(z)$ independent of t. However this does not work because the effect of $S(z)$ is then absorbed in the pressure as seen in (2.1). Therefore, we need to retain the concentration disturbance field Σ and instead choose to eliminate the eddy transport of concentration $J(\psi,\Sigma)$ after substituting (3.1) into (2.9). This elimination would

be justified if $J(\psi, \Sigma)$ were a much smaller quantity than other terms. But this does not necessarily hold in our numerical experiments in Section 2.3. Although no asymptotic justification is yet available, the numerical results of this model (given below) show qualitative similarity to those of the original system, and we adopt

$$\partial_t \Sigma + J(\psi, S_\delta) = \frac{1}{Le}\nabla^2 \Sigma \tag{3.2}$$

instead of (2.9), for the purpose of qualitative understanding the structure of the change in the convection patterns observed in the original system. $\langle \Sigma \rangle_x = 0$ always holds if it is satisfied at the initial time, and so we obtain $\langle S \rangle_x = S_\delta$ for any t. In the following, we treat δ as a time-independent fixed parameter, and consider a model system of (2.7), (2.8), (3.1) and (3.2) under the boundary conditions (2.4), (2.5) and (2.6). In this model, the width of the horizontally averaged transitional layer is constant for several values of δ, and we have a stationary state $\psi = 0$, $T = T_0(z) = (1/2)(1-z)$, $\Sigma = 0$ ($S = S_\delta(z)$). Hereafter, we employ the parameter values in (2.10) and also the initial conditions (2.11) and (2.12) for the model study, unless otherwise specified.

3.2 Linear stability problem of the stationary state

Because the coefficients appearing in the linearized equations (2.7), (2.8) and (3.2) do not depend on x and t, we can seek solutions in the following form:

$$\begin{aligned}
\psi(x,z,t) &= 0 &&+ \tilde{\Psi}(z)e^{ikx+\sigma t},\\
T(x,z,t) &= T_0(z) &&+ \tilde{\Theta}(z)e^{ikx+\sigma t},\\
\Sigma(x,z,t) &= 0 &&+ \tilde{\Sigma}(z)e^{ikx+\sigma t},
\end{aligned}$$

where $\sigma = r - i\omega$ is a complex constant, in which r and ω are the growth rate and the frequency, respectively. The linearized equations become

$$\sigma(D^2 - k^2)\tilde{\Psi} = -RaPrik(\tilde{\Theta} - B\tilde{\Sigma}) + Pr(D^2 - k^2)^2\tilde{\Psi}, \tag{3.3}$$

$$\sigma\tilde{\Theta} = ik(DT_0)\tilde{\Psi} + (D^2 - k^2)\tilde{\Theta}, \tag{3.4}$$

$$\sigma\tilde{\Sigma} = ik(DS_\delta)\tilde{\Psi} + \frac{1}{Le}(D^2 - k^2)\tilde{\Sigma}, \tag{3.5}$$

where $D = \frac{d}{dz}$. The boundary conditions of $\tilde{\Psi}$, $\tilde{\Theta}$ and $\tilde{\Sigma}$ derived from (2.4), (2.5), and (2.6) are written as

$$\tilde{\Psi}(\pm 1) = D\tilde{\Psi}(\pm 1) = \tilde{\Theta}(\pm 1) = D\tilde{\Sigma}(\pm 1) = 0. \tag{3.6}$$

Let $\tilde{\Theta}' \equiv i\tilde{\Theta}$ and $\tilde{\Sigma}' \equiv i\tilde{\Sigma}$, then by substituting them into (3.3), (3.4), and (3.5) we obtain

$$\sigma \begin{pmatrix} D^2-k^2 & 0 & 0 \\ 0 & 1 & 0 \\ 0 & 0 & 1 \end{pmatrix} \begin{bmatrix} \tilde{\Psi} \\ \tilde{\Theta}' \\ \tilde{\Sigma}' \end{bmatrix} = \begin{pmatrix} Pr(D^2-k^2)^2 & -RaPrk & RaPrBk \\ -k(DT_0) & D^2-k^2 & 0 \\ -k(DS_\delta) & 0 & \dfrac{1}{Le}(D^2-k^2) \end{pmatrix} \begin{bmatrix} \tilde{\Psi} \\ \tilde{\Theta}' \\ \tilde{\Sigma}' \end{bmatrix}. \tag{3.7}$$

The boundary conditions (3.6) become

$$\tilde{\Psi}(\pm 1) = D\tilde{\Psi}(\pm 1) = \tilde{\Theta}'(\pm 1) = D\tilde{\Sigma}'(\pm 1) = 0. \tag{3.8}$$

For the given Ra, Le, Pr, B, k and δ, (3.7) and (3.8) setup a generalized eigenvalue problem of a linear operator with respect to an eigenvalue σ and an eigenstate $[\tilde{\Psi}, \tilde{\Theta}', \tilde{\Sigma}']^T$. Note that the eigenvalues of (3.7) and (3.8) are real, or pairs of complex conjugates with complex conjugate eigen functions, because the coefficients of the equations are all real.

The variables $\tilde{\Psi}(z)$, $\tilde{\Theta}'(z)$ and $\tilde{\Sigma}'(z)$ are discretized by the finite difference method, using 1001 equally spaced grid points. The generalized eigenvalue problem of (3.7) and (3.8) is solved by LAPACK (http://www.netlib.org/lapack/). We adopt the same parameter values for Pr, Le, and B as in (2.10) in most of this section, except in a part of Section 3.4, where B is varied over the range $1 \le B \le 10$. We seek neutral curves by solving the equation $r = 0$ using the binary search method, changing the wave number k from 1 to 4 in steps of 0.05.

3.3 Neutral modes

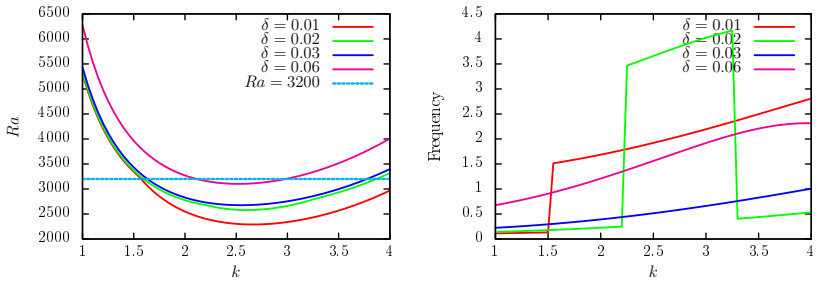

Figure 3.1: Neutral curves and frequency at $\delta = 0.01$ (red solid curve), 0.02 (green solid curve), 0.03 (blue solid curve), and 0.06 (magenta solid curve). The critical wave number and Rayleigh number (k_c, Ra_c) are $(2.65, 2290.47)$ at $\delta = 0.01$, $(2.60, 2578.97)$ at $\delta = 0.02$, $(2.55, 2675.78)$ at $\delta = 0.03$, and $(2.50, 3102.34)$ at $\delta = 0.06$. The critical points are under the line of $Ra = 3200$ (cyan dashed line), as adopted in Section 2.3, when $\delta \lesssim 0.06$.

Neutral curves at $\delta = 0.01$, 0.02, 0.03, and 0.06 are shown in the left panel of Fig. 3.1. The curves move upward and the critical wave number decreases as

the width of the transient layer δ increases. All the neutral modes obtained here are oscillatory ($\omega \neq 0$) as shown in the right panel of Fig. 3.1. Staircase-like variations observed in the frequency graphs for $\delta = 0.01$ and 0.02 are due to interchange of the viscous and thermal coupling modes. The larger frequency is for the viscous coupling mode. The line of the Rayleigh number ($Ra = 3200$) adopted in Section 2.3 is also drawn in the left panel of Fig. 3.1. The critical Rayleigh numbers are lower than 3200 when $\delta \lesssim 0.06$. This implies that the stationary state is unstable with respect to infinitesimal disturbances when $Ra = 3200$ and $\delta \lesssim 0.06$.

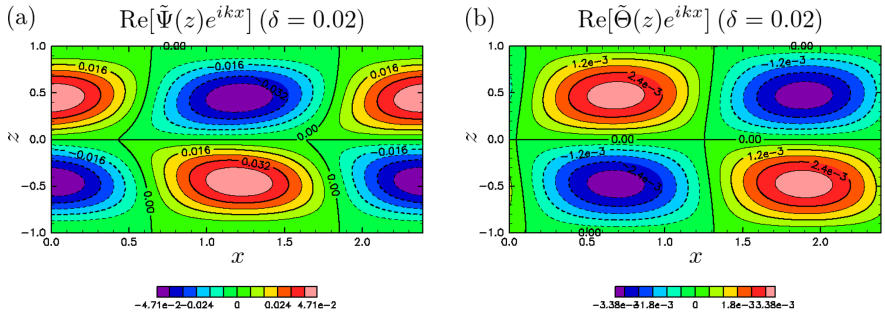

Figure 3.2: Critical mode at $\delta = 0.02$: (a) the stream function and (b) the temperature deviation. This convection pattern is identified as viscous coupling. The critical frequency ω_c is -3.736, and the propagation velocity is $\omega_c/k_c = -1.44$.

Figure 3.2 shows the critical mode at $\delta = 0.02$ with negative ω. Vortices at the same horizontal position are observed to rotate in the direction opposite to each other in Fig. 3.2 (a). The disturbance of the temperature shown in Fig. 3.2 (b) has opposite signs in the upper and lower layers, indicating that the convection pattern is viscous coupling. The critical frequency ω_c is -3.736, and the propagation velocity is $\omega_c/k_c = -1.44$. There exists another critical mode with $\omega_c = 3.736$ arising from the reflectional symmetry ($x \leftrightarrow -x$). Note that the horizontal propagation is an artifact not observed in the original system.

We can see from Fig. 3.2 that the critical mode satisfies the following symmetry:

$$\begin{bmatrix} \tilde{\Psi}(-z) \\ \tilde{\Theta}(-z) \\ \tilde{\Sigma}(-z) \end{bmatrix} = - \begin{bmatrix} \tilde{\Psi}(z) \\ \tilde{\Theta}(z) \\ \tilde{\Sigma}(z) \end{bmatrix}. \tag{3.9}$$

This symmetric property is consistent with the linearized equations (3.3), (3.4), and (3.5) and the boundary conditions (3.6). In this thesis, we call (3.9) the "symmetry of viscous coupling", and the mode accompanying it the "viscous coupling mode."

Figure 3.3 shows the critical mode at $\delta = 0.03$ with negative ω. Vortices at the same horizontal position are observed to rotate in the same direction in Fig. 3.3 (a). The disturbance of the temperature displayed in Fig. 3.3 (b) has

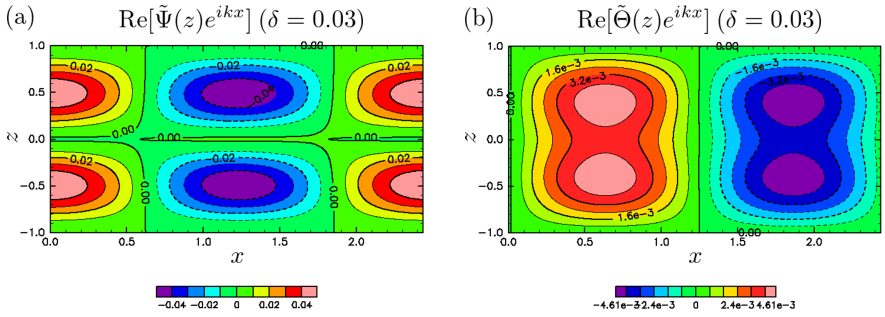

Figure 3.3: The critical mode at $\delta = 0.03$: (a) the stream function and (b) the temperature deviation. Vortices at the same horizontal position rotate in the same direction. This convection pattern is identified as thermal coupling. The critical frequency ω_c is -0.529, and the propagation velocity is $\omega_c/k_c = -0.21$, which is much slower than that of the critical mode at $\delta = 0.02$.

the same sign in the upper and lower layers. This convection pattern is thermal coupling. The critical frequency of this mode ω_c is -0.529, and the propagation velocity is $\omega_c/k_c = -0.21$, which is much lower than that of the critical mode at $\delta = 0.02$. In this case another critical mode arising from the reflectional symmetry ($x \leftrightarrow -x$) exists with $\omega_c = 0.529$.

We can see from Fig. 3.3 that the critical mode satisfies the following symmetry:

$$\begin{bmatrix} \tilde{\Psi}(-z) \\ \tilde{\Theta}(-z) \\ \tilde{\Sigma}(-z) \end{bmatrix} = \begin{bmatrix} \tilde{\Psi}(z) \\ \tilde{\Theta}(z) \\ \tilde{\Sigma}(z) \end{bmatrix}. \tag{3.10}$$

This symmetric property is also consistent with the linearized equations (3.3), (3.4), (3.5), and the boundary conditions (3.6). We call (3.10) the "symmetry of thermal coupling," and the mode accompanying it the "thermal coupling mode."

At other values of $\delta \leq 0.1$, the critical modes have the symmetry of viscous coupling when $\delta \lesssim 0.02$, while the critical modes have the symmetry of thermal coupling when $\delta \gtrsim 0.02$. Therefore the symmetry of the critical mode changes at $\delta \approx 0.02$.

Rasenat *et al.* [16] and Le Bars & Davaille [11] performed linear stability analysis of the infinitesimal transition layer, and found only the viscous coupling mode at criticality when the vertical lengths of the layers and the physical properties of the fluids in the two layers were the same, except for the densities. Our analysis found that the viscous coupling mode remains as a critical mode when the transitional layer has a finite width less than about 0.02. This implies that the width of the transitional layer is crucial for determining the structure of convection in two layer miscible fluids.

3.4 Unstable modes at $Ra = 3200$

Here, we investigate unstable modes at $Ra = 3200$, which is the value used in Section 2.3, and discuss the behavior found in Section 2.3 using linear instability.

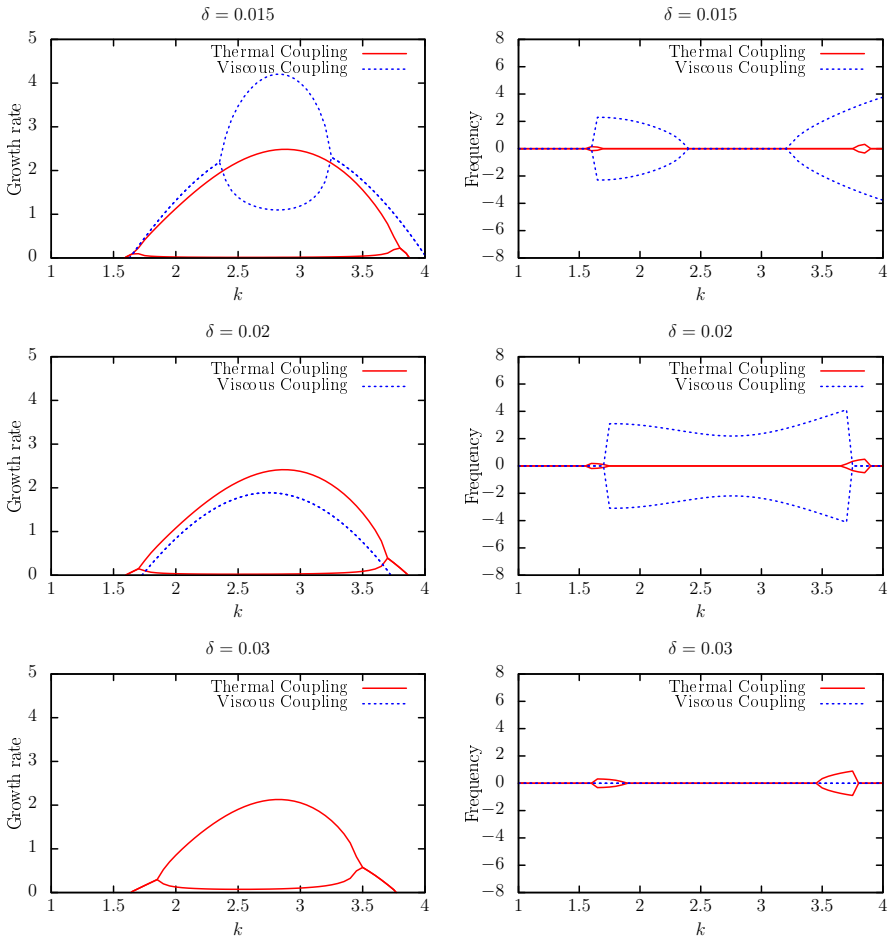

Figure 3.4: Growth rate and frequency of unstable thermal coupling modes (red solid curve) and of viscous coupling modes (blue dashed curve) for three values of δ at $Ra = 3200$. The step width of the wave number k is 0.05.

The growth rate and frequency of unstable modes at several values of δ are shown in Fig. 3.4, where the wave number k varies in steps of 0.05. When $\delta = 0.015$, the most unstable viscous coupling mode, whose wave number is $k = 2.85$ and is non-oscillatory, has a higher growth rate than that of the most unstable thermal coupling mode, whose wave number is $k = 2.9$ and is oscillatory (top row of Fig. 3.4). At $\delta = 0.02$, unstable oscillatory viscous coupling modes and non-oscillatory thermal coupling modes exist, but the growth rate of the

most unstable viscous coupling mode at $k = 2.75$ is less than that of the most unstable thermal coupling mode at $k = 2.85$ (middle row of Fig. 3.4). Thus the most unstable mode changes from viscous coupling to thermal coupling when $0.015 < \delta < 0.02$. At $\delta = 0.03$, all viscous coupling modes are stable, while unstable thermal coupling modes exist (bottom row of Fig. 3.4). Both viscous coupling modes and thermal coupling modes are found to be stable when $\delta = 0.07$ (not shown).

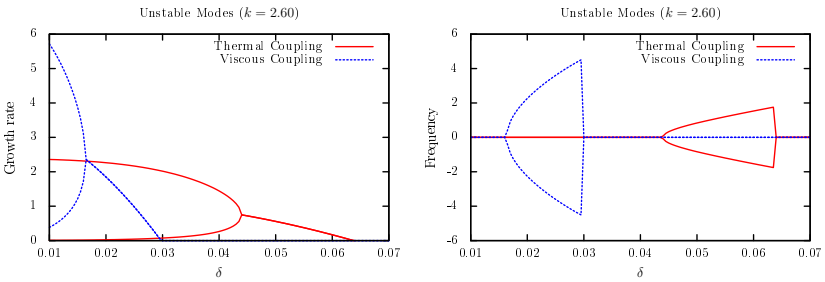

Figure 3.5: Growth rate and frequency of unstable thermal coupling modes (red solid curve) and viscous coupling modes (blue dashed curve) at $k = 2.60$ and $Ra = 3200$. The step width of δ is 0.0005.

Next, we consider the dependence of the growth rate and the frequency on the width of the transition layer, δ, taking fixed values of $k = 2.60$, $Ra = 3200$, and $L_x = \dfrac{4\pi}{2.60}$, which were adopted in Section 2.3. The growth rate and frequency of unstable modes are shown in Fig. 3.5. Unstable thermal coupling modes exist for $\delta < 0.064$, and unstable viscous coupling modes exist for $\delta < 0.03$. Thermal coupling modes have two branches of growth rates for $\delta < 0.044$, while only a single branch of growth rate is found for $\delta > 0.044$. The thermal coupling modes for $\delta < 0.044$ are stationary modes, that is, $\omega = 0$, while those for $\delta > 0.044$ are oscillatory modes, that is, $\omega \neq 0$. A similar behavior of viscous coupling modes is found at $\delta = 0.016$. The viscous coupling modes for $\delta < 0.016$ are stationary modes, while those for $\delta > 0.016$ are oscillatory modes. The most unstable mode exchanges at $\delta = 0.017$: the most unstable mode is the viscous coupling mode for $\delta < 0.017$ while the most unstable mode is the thermal coupling mode for $\delta > 0.017$. The frequency values of the oscillations before and after $t = 2.0$ in the numerical experiment shown in Section 2.3 are 4.6 and 2.5, respectively. These are comparable to the frequencies of the oscillatory viscous and thermal coupling mode at $\delta > 0.02$ and $\delta > 0.044$, respectively.

Figure 3.6 shows the kind of the symmetry (viscous/thermal coupling) and the time dependence (stationary/oscillatory) of the most unstable mode of the buoyancy number, B ($1 \leq B \leq 10$), which expresses the density contrast, and the transitional layer width δ ($0.01 \leq \delta \leq 0.1$) with $k = 2.60$ and $Ra = 3200$. As δ increases from 0.01 to 0.10 for $B > 2$, the most unstable mode changes from stationary viscous coupling mode to oscillatory viscous coupling

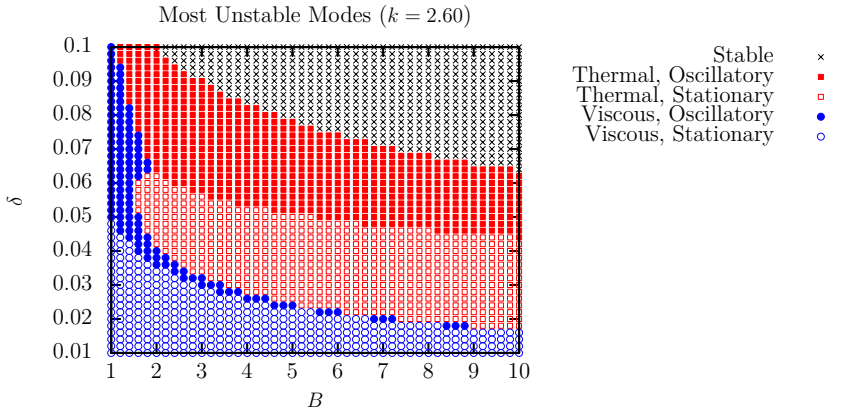

Figure 3.6: Types of the most unstable modes for $0.01 \leq \delta \leq 0.1$ and $1 \leq B \leq 10$: stable modes (black crosses), thermal coupling modes (red solid and open squares) and viscous coupling modes (blue solid and open circles). Filled symbols represent oscillatory modes, and hollow ones represent stationary convections.

mode, stationary thermal coupling mode, oscillatory thermal coupling mode, and stable mode in that order.

In the nonlinear simulation described in Section 2.3, the convection starts in the form of the viscous coupling pattern as long as the width of the transitional layer δ is small. However, as time proceeds, the width of transitional layer δ gradually increases while the mixing effect of convection is not strong enough to appreciably change the density contrast between the upper and lower layers. According to Fig. 3.6, the increase of δ corresponds to the transition of the convection pattern from viscous coupling to thermal coupling. Actually, this pattern transition is observed in the numerical experiment described in Section 2.3, consistent with Fig. 3.6.

3.5 Asymptotic behavior of nonlinear states after a long time integration

In all cases in our numerical study, the numerical solutions up to $t = 100$ are observed to approach time periodic solutions asymptotically.

Figure 3.7 shows the stream function ψ, the temperature deviation Θ and the concentration deviation Σ, numerically obtained in the nonlinear simulation of the model at $t = 100$ for $\delta = 0.015$. Two streets of vortex arrays are observed, where the vortices in the upper street rotate in the direction opposite to that of the lower vortices just below them. Similar to the numerical simulations discussed in Section 2.3, the signs of the temperature deviation are opposite in

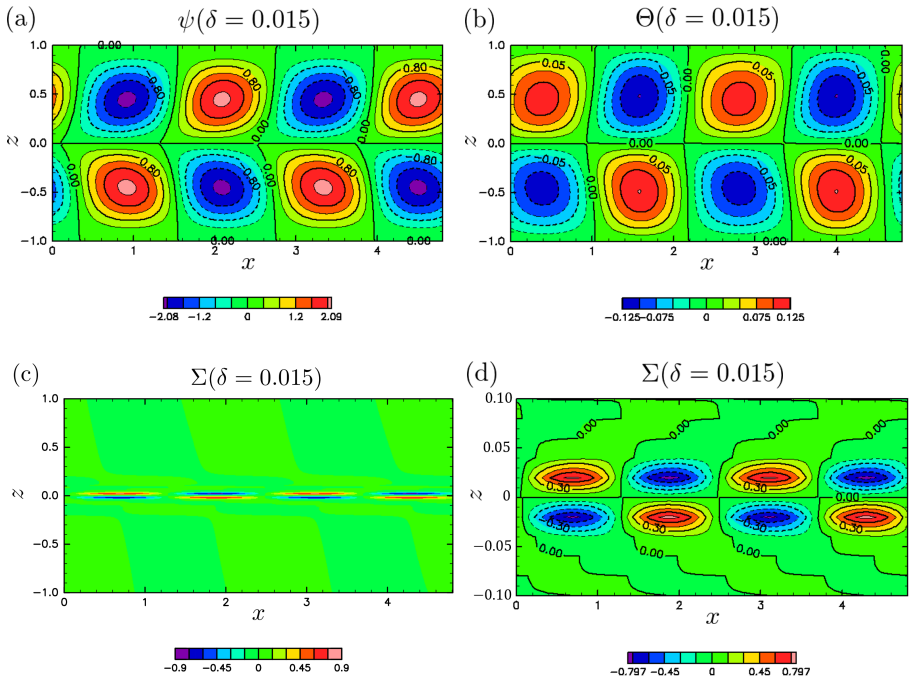

Figure 3.7: Snapshots of a time periodic asymptotic state at $t = 100$ for $\delta = 0.015$; (a) the stream function ψ, (b) the temperature deviation Θ and (c), (d) the concentration deviation, where (d) is made by enlarging $-0.1 \leq z \leq 0.1$ of (c). The convection is identified as viscous coupling.

the upper and lower vortices. The convection is therefore viscous coupling. This convection pattern moves in the negative x direction, with the two arrays of the convection pattern remaining unchanged. This solution is thus a traveling wave with a velocity of about -1.51. The model system as well as the original system has a reflectional symmetry with respect to the vertical axis at $x = 0$, and therefore the traveling wave solution in the positive x direction also exists. The initial condition determines which traveling wave is actually observed. Over the course of time development from the initial condition, the convection maintains itself for some time, and decreases gradually to an almost quiescent state, and again starts rotation in the direction opposite to the initial convection pattern. This process continues in parallel in both layers. After the repeated reversal of the convection direction, the convection finally converges to the traveling wave moving in the negative x direction with a velocity of about -1.51.

From Fig. 3.7, we observe that the system is invariant to the transformation $\mathscr{F}_{\text{vis}}$ defined by

$$\mathscr{F}_{\text{vis}} \begin{bmatrix} \psi(x,z) \\ \Theta(x,z) \\ \Sigma(x,z) \end{bmatrix} = \begin{bmatrix} -\psi(x,-z) \\ -\Theta(x,-z) \\ -\Sigma(x,-z) \end{bmatrix},$$

which we call the "viscous coupling transformation". Actually, this may give a formal definition of the "viscous coupling" solution.

In contrast, Fig. 3.8 shows the asymptotic state for a slightly larger transitional layer width $\delta = 0.02$ where the upper and lower vortices are observed to rotate in the same direction, and the signs of the temperature deviation and the concentration deviation are observed to be the same in the upper and lower vortices. Thus the convection is thermal coupling. As time proceeds, this thermal coupling convection experiences a process similar to that of viscous coupling convection, and finally converges to a traveling wave moving in the positive x direction with a velocity of about 0.59.

Similar to Fig. 3.7, the solution of the thermal coupling state shown in Fig. 3.8 is observed to be invariant under the transformation $\mathscr{F}_{\text{therm}}$ defined by

$$\mathscr{F}_{\text{therm}} \begin{bmatrix} \psi(x,z) \\ \Theta(x,z) \\ \Sigma(x,z) \end{bmatrix} = \begin{bmatrix} -\psi\left(x - \dfrac{L_x}{4}, -z\right) \\ -\Theta\left(x - \dfrac{L_x}{4}, -z\right) \\ -\Sigma\left(x - \dfrac{L_x}{4}, -z\right) \end{bmatrix},$$

which we call the "thermal coupling transformation". Note that, we have included the horizontal translation of $\dfrac{L_x}{4}$ because, in our simulation, four convection cells were observed in the computation domain, and that these symmetries with respect to $\mathscr{F}_{\text{vis}}$ and $\mathscr{F}_{\text{therm}}$ are conserved respectively in the time development of (2.7), (2.8), and (3.2) and the boundary conditions (2.4), (2.5), and (2.6). This transformation may provide a formal definition of the "thermal coupling" solution, similar to the viscous coupling case.

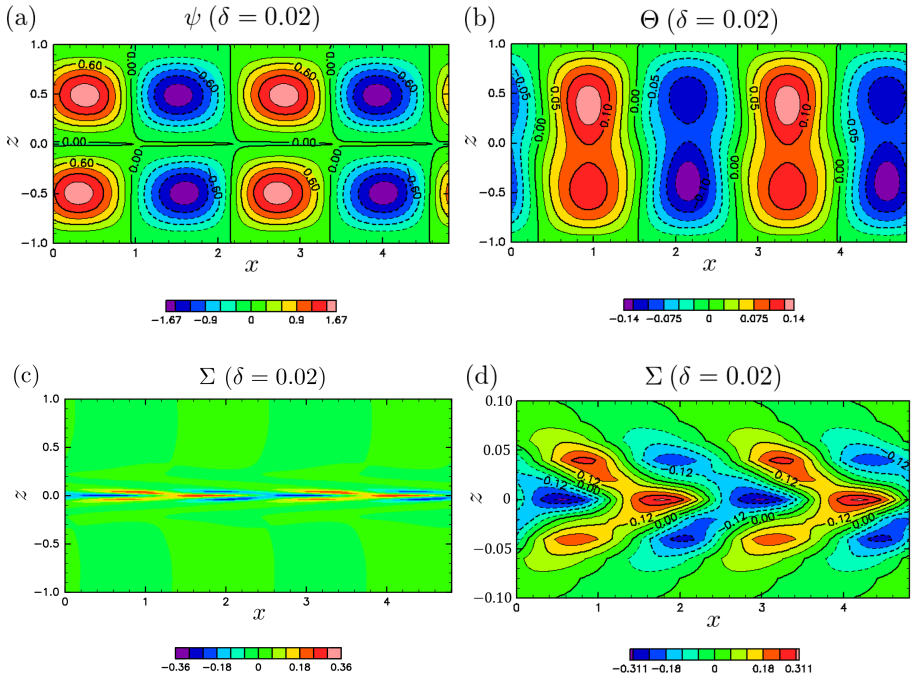

Figure 3.8: Snapshots of a time periodic asymptotic state at $t = 100$ for $\delta = 0.02$: (a) the stream function ψ, (b) the temperature deviation Θ and (c), (d) the concentration deviation, where (d) is made by enlarging $-0.1 \leq z \leq 0.1$ of (c). The convection is identified as thermal coupling.

In each case of $\delta = 0.03, 0.04, 0.05$, and 0.06, the asymptotic state is observed to be a traveling wave with thermal coupling symmetry, while the flow decays to the quiescent state for $\delta = 0.07$.

In summary, the time periodic asymptotic state of viscous coupling is observed for $\delta \lesssim 0.015$, and that of thermal coupling is observed for $\delta \gtrsim 0.02$.

3.6 Projections to viscous coupling and thermal coupling function spaces

We now define projection operators for viscous coupling and thermal coupling function spaces. We introduce an inner product of $[\psi_1(x,z), \Theta_1(x,z), \Sigma_1(x,z)]^T$ and $[\psi_2(x,z), \Theta_2(x,z), \Sigma_2(x,z)]^T$ as

$$\left(\begin{bmatrix} \psi_1 \\ \Theta_1 \\ \Sigma_1 \end{bmatrix}, \begin{bmatrix} \psi_2 \\ \Theta_2 \\ \Sigma_2 \end{bmatrix} \right) = \int_0^{L_x} \int_{-1}^{1} (\psi_1\psi_2 + \Theta_1\Theta_2 + \Sigma_1\Sigma_2) dz dx,$$

where we assume a real Hilbert space as ψ, Θ, and Σ are real variables. For a thermal convection $[\psi(x,z), \Theta(x,z), \Sigma(x,z)]^T$, the orthogonal projection operator to the viscous coupling space is defined as

$$\mathscr{P}_{\text{vis}} \begin{bmatrix} \psi(x,z) \\ \Theta(x,z) \\ \Sigma(x,z) \end{bmatrix} = \begin{bmatrix} \frac{1}{2}\left(\psi(x,z) - \psi(x,-z)\right) \\ \frac{1}{2}\left(\Theta(x,z) - \Theta(x,-z)\right) \\ \frac{1}{2}\left(\Sigma(x,z) - \Sigma(x,-z)\right) \end{bmatrix},$$

which clearly leaves the viscous coupling convection invariant. Also, the projection operator orthogonal to the thermal coupling space is given by

$$\begin{aligned} &\mathscr{P}_{\text{therm}} \begin{bmatrix} \psi(x,z) \\ \Theta(x,z) \\ \Sigma(x,z) \end{bmatrix} \\ &= \begin{bmatrix} \frac{1}{4}\left(\psi(x,z) - \psi\left(x + \frac{L_x}{4}, -z\right) + \psi\left(x + \frac{2L_x}{4}, z\right) - \psi\left(x + \frac{3L_x}{4}, -z\right)\right) \\ \frac{1}{4}\left(\Theta(x,z) - \Theta\left(x + \frac{L_x}{4}, -z\right) + \Theta\left(x + \frac{2L_x}{4}, z\right) - \Theta\left(x + \frac{3L_x}{4}, -z\right)\right) \\ \frac{1}{4}\left(\Sigma(x,z) - \Sigma\left(x + \frac{L_x}{4}, -z\right) + \Sigma\left(x + \frac{2L_x}{4}, z\right) - \Sigma\left(x + \frac{3L_x}{4}, -z\right)\right) \end{bmatrix}, \end{aligned}$$

which also keeps the thermal coupling convection invariant. We call the ranges of these operators, $\mathscr{P}_{\text{vis}}$ and $\mathscr{P}_{\text{therm}}$, the viscous coupling space and the thermal coupling space, respectively. Note that these spaces are invariant under nonlinear time development (see Appendix A.1). The viscous coupling and the thermal coupling spaces are not orthogonal to each other, because their intersection includes a nontrivial linear space. However, if we take the orthogonal

complements of the linear space respectively in the viscous coupling space and the thermal coupling space, these orthogonal complements are mutually orthogonal (see Appendix A.2). This observation enables us to classify the solution attractors into viscous coupling and thermal coupling attractors in the next section.

3.7 Time integration of viscous coupling and thermal coupling convections

When the convection field is in the viscous coupling or thermal coupling spaces, it remains so as time passes. We found that these two types of convections are realized in the numerical simulations shown in Section 2.3, and they are considered to be typical convection states that may exhibit attractor-like behavior in the solution space. Therefore, we now search for the solutions in these spaces in some detail. We stress that we should then suppress the instability that makes the solution escape from these spaces. To do so, we project the solution to the relevant space at each time step of the numerical integration.

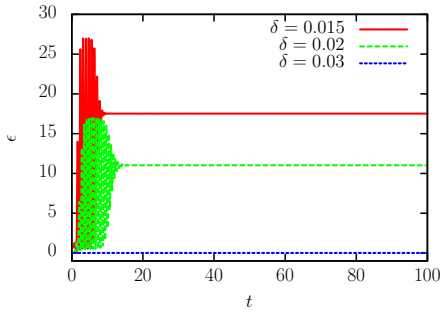

Figure 3.9: Time series of the kinetic energy ϵ per unit volume for the case of viscous coupling for $\delta = 0.015, 0.02$, and 0.03.

The kinetic energy ϵ per unit volume for the case of the viscous coupling for $\delta = 0.015, 0.02$ and 0.03 is shown in Fig. 3.9, where ϵ is defined by

$$\epsilon(t) \equiv \frac{1}{2L_x} \int_0^{L_x} \int_{-1}^{1} \frac{1}{2} |\boldsymbol{u}(x, z, t)|^2 \, dz dx.$$

In all cases, the kinetic energy converges fairly well to a constant value. The convection pattern is found to approach the traveling wave for $\delta = 0.015$ and 0.02, and it decays to the quiescent state for $\delta = 0.03$.

In the case of thermal coupling symmetry, the kinetic energies ϵ per unit volume for $0.015 \leq \delta \leq 0.06$ are shown in Fig. 3.10 (a). We plot longer time integrations until $t = 200$ for the cases of $\delta = 0.015$ and 0.06 in Fig. 3.10 (b). In all cases, the kinetic energy converges fairly well to a constant value, and we see that the convections are found to converge to the traveling waves.

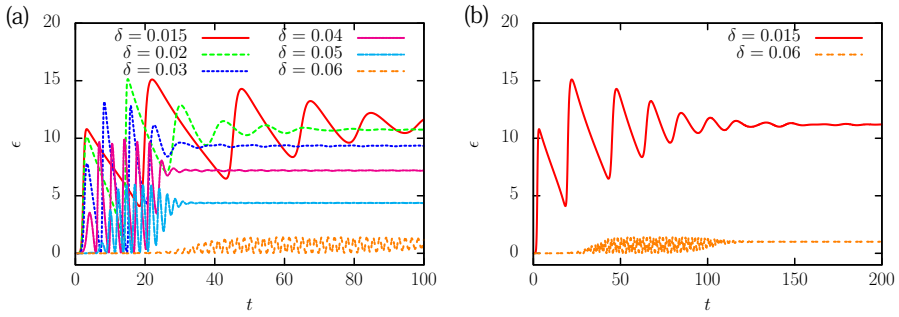

Figure 3.10: Time series of the kinetic energy ϵ per volume for the case of thermal coupling for (a) $\delta = 0.015, 0.02, 0.03, 0.04, 0.05$ and 0.06 until $t = 100$, and (b) $\delta = 0.015$ and 0.06 until $t = 200$.

Therefore, the asymptotic states with the viscous coupling and thermal coupling symmetries are found to coexist for $\delta = 0.015$ and 0.02. However, as discussed at the end of Section 3.6, the function spaces of viscous coupling and thermal coupling have a nontrivial intersection. Now, we define subspaces of these spaces that are orthogonal to each other, to confirm that the attracting set (which may be attractors) of the viscous coupling solutions contain a subset that is not in the attracting set of the thermal coupling solutions, and vice versa.

For a convection $[\psi, \Theta, \Sigma]^T$, we define $\psi_{\rm vis}$, $\Theta_{\rm vis}$ and $\Sigma_{\rm vis}$ by

$$\begin{bmatrix} \psi_{\rm vis} \\ \Theta_{\rm vis} \\ \Sigma_{\rm vis} \end{bmatrix} = (\mathscr{P}_{\rm vis} - \mathscr{P}_{\rm vis}\mathscr{P}_{\rm therm}) \begin{bmatrix} \psi \\ \Theta \\ \Sigma \end{bmatrix}.$$

Similarly, we define $\psi_{\rm therm}$, $\Theta_{\rm therm}$ and $\Sigma_{\rm therm}$ by

$$\begin{bmatrix} \psi_{\rm therm} \\ \Theta_{\rm therm} \\ \Sigma_{\rm therm} \end{bmatrix} = (\mathscr{P}_{\rm therm} - \mathscr{P}_{\rm vis}\mathscr{P}_{\rm therm}) \begin{bmatrix} \psi \\ \Theta \\ \Sigma \end{bmatrix}.$$

Then, $(\psi_{\rm vis}, \Theta_{\rm vis}, \Sigma_{\rm vis})$ and $(\psi_{\rm therm}, \Theta_{\rm therm}, \Sigma_{\rm therm})$ respectively belong to the viscous coupling and thermal coupling spaces, and they are both orthogonal to the intersection of the two spaces.

Now, we define two kinds of kinetic energy as

$$\epsilon_{\rm vis}(t) \equiv \frac{1}{2L_x}\int_0^{L_x}\int_{-1}^{1} \frac{1}{2}|\boldsymbol{u}_{\rm vis}(x,z,t)|^2\, dzdx,$$
$$\epsilon_{\rm therm}(t) \equiv \frac{1}{2L_x}\int_0^{L_x}\int_{-1}^{1} \frac{1}{2}|\boldsymbol{u}_{\rm therm}(x,z,t)|^2\, dzdx,$$

where

$$\boldsymbol{u}_{\rm vis} = \begin{pmatrix} \partial_z\psi_{\rm vis} \\ -\partial_x\psi_{\rm vis} \end{pmatrix}, \quad \boldsymbol{u}_{\rm therm} = \begin{pmatrix} \partial_z\psi_{\rm therm} \\ -\partial_x\psi_{\rm therm} \end{pmatrix}.$$

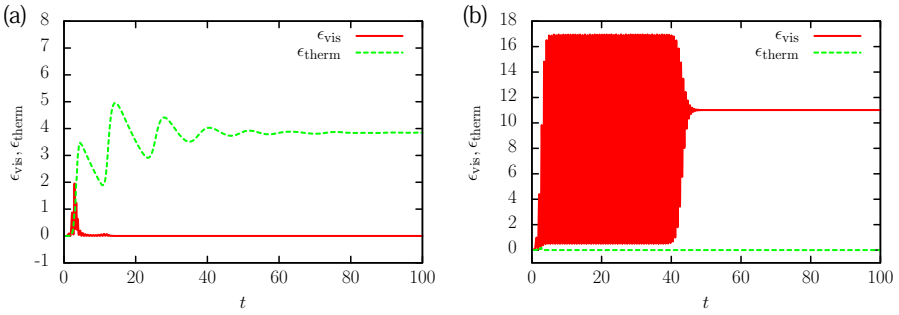

Figure 3.11: Time series of the kinetic energy $\epsilon_{\rm vis}$ and $\epsilon_{\rm therm}$ for $\delta = 0.02$. (a) and (b) are two realizations under different initial conditions: (a) corresponds to the case shown in Fig. 3.8, and (b) is a case with an initial condition different from that of (a).

Then $\epsilon_{\rm therm} = 0$ holds if the convection pattern has the symmetry of the viscous coupling, and $\epsilon_{\rm vis} = 0$ holds when the convection pattern has the symmetry of the thermal coupling.

The time series of the kinetic energy $\epsilon_{\rm vis}$ and $\epsilon_{\rm therm}$ for $\delta = 0.02$ under two different initial conditions are shown in Fig. 3.11, where (a) corresponds to the flow shown in Fig. 3.8, and (b) is a case with an initial condition different from that of (a). In the case of (a), $\epsilon_{\rm therm} \gg \epsilon_{\rm vis} \approx 0$ holds and so the asymptotic state is thermal coupling and has a non-viscous coupling component, which is consistent with Fig. 3.8. Conversely, $\epsilon_{\rm vis} \gg \epsilon_{\rm therm} \approx 0$ holds in the case of (b) and so the asymptotic state is viscous coupling and has a non-thermal coupling component. Therefore, an asymptotic state with either symmetry can be realized depending on the initial conditions. In other words, attractors with viscous coupling and thermal coupling convection patterns coexist at $\delta = 0.02$.

In summary, the attractors behave as follows:

(a) For sufficiently small δ, $0 < \delta \lesssim 0.02$, attractors exist with both viscous coupling and thermal coupling convection patterns.

(b) For a larger δ, $0.03 \lesssim \delta \lesssim 0.06$, only attractors with the thermal coupling convection pattern exist.

(c) For a sufficiently large δ, $0.07 \lesssim \delta$, all the fluid motion decays to the quiescent state.

Therefore, the change of convection patterns observed in numerical simulations in Section 2.3 may correspond to the disappearance of the attractor of viscous coupling in the model system.

Chapter 4

Discussions and Conclusions

Many methods have been exploited to explain the mechanism of structure formation in flows, including the linear stability analysis, the bifurcation theory, and the explanation as a dynamical system. These standard approaches assume that the system has a steady or time-periodic solution. If the system under analysis does not have such a solution, one has to develop a different method. To propose some solution to this problem, we treated a miscible two-layer thermal convection system as an example. We focused on the transition of convection patterns from viscous coupling to thermal coupling, which we observed in numerical simulations.

We first describe and discuss the results of analyses on the two-layer thermal convection system in Section 4.1. After that, in Section 4.2, we discuss the possibility of the modeling approach to transient phenomena in general.

4.1 Modeling convection system with two miscible layers

In chapters 2 and 3, we reported our study of the transient behavior of double diffusive convection where the upper and lower fluids are miscible with each other. Numerical experiments showed two patterns of convection, namely viscous coupling and thermal coupling. Viscous coupling took place in the initial convection stage, and was replaced by thermal coupling as the width of the transitional layer increased.

These two patterns have been investigated in immiscible two-layer thermal convection systems. Because immiscible fluids have a definite interface between them, the system has a stationary state with a fixed horizontal interface, which enables us to apply the standard methods. In miscible fluids, however, even if the interface between them exists initially, it becomes unclear by the diffusion of concentration. Then the system has only a transitional layer in which the concentration continuously changes. Therefore the thermal convection system of two miscible layers does not have a stationary state with a two-layered structure,

which prevents the standard methods from applying.

To cope with this problem and describe a possible mechanism of the change in convection patterns, we introduced a model in which the width of the transitional layer between the upper and lower layers (δ) is kept constant in the horizontal average. Both the linear stability of a stationary state of the model and nonlinear time periodic solutions implied that viscous coupling is preferred when the width of the transitional layer δ is small, and thermal coupling is preferred when δ is large. Furthermore the transition from viscous coupling to thermal coupling was observed at $\delta \approx 0.02$ in all cases.

First, we investigated the linear stability of a stationary state of the model. In our calculation, the critical Rayleigh number Ra_c varied from 2290 ($\delta = 0.01$) to 3102 ($\delta = 0.06$). The convection pattern of the critical mode was observed to be viscous coupling when δ was small, and thermal coupling when δ was large. The convection pattern of the most unstable mode at $Ra = 3200$ also changed from viscous coupling for small δ to thermal coupling for large δ. This property was also observed for different concentration contrasts between the two layers except when the concentration difference was very small.

Rasenat *et al.* [16] performed linear stability analysis of the steady state of a two-layer thermal convection system of immiscible fluids (thus with an infinitesimal transitional layer), and showed that the viscous coupling mode is preferred when fluid properties in both layers are nearly equal. Le Bars & Davaille [11] experimentally and analytically studied the cases of immiscible fluids with different density contrasts between the two layers. They studied the linear stability of the stationary state under the assumption of an infinitesimal transitional layer and found only the viscous coupling mode for the marginal mode.

In our linear stability analysis, which focused on density contrast $B > 1$, the viscous coupling mode is preferred when the width of the transitional layer is small, while the thermal coupling mode is preferred in the large width case. The model proposed in this thesis not only reproduces the emergence of the viscous coupling convection for small transitional layer widths, but also shows the transition from viscous coupling to thermal coupling convection when the transitional layer width increases. This implies that the width of the transitional layer crucially affects the convection structure in two layer miscible fluids. Note that, to our knowledge, the previous theoretical studies treated only the case of a transitional layer with infinitesimal thickness (e.g. [11, 13]).

Oscillatory modes were found by Rasenat *et al.* [16], but they were not the critical modes. Nepomnyanshchy *et al.* [14] found oscillatory critical modes by introducing the thermo-capillary effect of the interface. In the present model study, oscillatory critical modes also arise when the transitional layer has a finite width. Eventually, numerical simulations of the original system of equations showed that the convection becomes oscillatory or time-dependent when the transitional layer width gradually increases.

In the linear stability analysis in the model system, we found that viscous coupling transitions to thermal coupling as the width of the transitional layer increases at various density contrasts between the two layers.

In contrast, a transition from the thermal coupling state to the viscous coupling state was observed in a laboratory experiment[25]. This may be explained by the thickness of the transition layer around the interface between the upper and lower layers. It has been reported that the observed boundary layer around the interface is fairly thick in the thermal coupling state, while in the viscous coupling state, the boundary layer becomes thinner than that in the thermal coupling state. If we interpret the thickness of the boundary layer as the thickness of the transition layer of the horizontally averaged density profile δ, these characteristics are consistent with our linear stability analyses where viscous (thermal) coupling becomes dominant at small (large) δ.

Next, in long time integration of the model we found that in the case of the small width of the transitional layer the flow approaches a time periodic convection whose pattern is viscous coupling, while in the case of the large width it approaches the time periodic thermal coupling convection. These model results are consistent with the numerical observation in the original system where the viscous coupling convection is realized when the width of the transitional layer is small, and the thermal coupling convection emerges when the width becomes large. Furthermore, time periodic solutions whose convection patterns were viscous coupling and thermal coupling were found to coexist when the width of the transitional layer was neither very large nor zero.

4.2 Modeling approach to transient phenomena in general

We discuss what kind of phenomena other than the convection in two-layer fluids might be suitable for our modeling approach, after reviewing the features of the method.

As described in the previous section, we proposed a method to construct a model in which the width of the transitional layer is fixed in the horizontal mean. The standard approaches were applicable to this system because it has a stationary state with a two-layer structure. The results of them were consistent with the behaviors of the original system.

We constructed the model by neglecting a part of the nonlinear terms of the basic equation. However, justifying this operation is not obvious, even though the resulting behavior resembled the original system. For example, if the neglected term was smaller than the other terms, it could be justified. Unfortunately, this criterion did not necessarily hold in our numerical experiment in 2.3. Another idea for justification is to compare the structures of the solution spaces. Specifically, this idea is to evaluate whether a continuous connection of the structures of the solution spaces of the model with different δ-s can well approximate the structure of the solution space of the original system. First, calculate the time development of the original system from the initial state on the attracting set of the model system. Second, evaluate the distance between the state and the attracting set of the model system. That is, measure the

width of the transitional layer of the flow state δ, and compare the state with the attracting set of the model system with the transitional layer width δ. If the distances are evaluated to be small in some sense, the structures of the model system can be considered as an approximation to the original system.

Finally, we discuss what kind of systems can be analyzed by similar methods to ours. Our method gave an error function as a "transient base field" of concentration. We deformed the basic equations so that the horizontal mean of the displacement from the "transient base field" at a fixed time is always zero. A similar method may be applied if the system can be assumed to have a "transient base field" concretely. The procedure is as follows:

(1) Fix a "transient base field" at a certain time and decompose the state into the basic field and displacement.

(2) Substitute them into the basic equations and derive the time evolution equations of the displacement.

(3) Deform or neglect some terms of the equations so that some spatial average of the displacement is always zero.

In the model created by the above procedure, the trajectory of the solution is bounded around a fixed "transient base field." Step (3) is the most nontrivial because one has to consider, depending on individual systems, what kind of spacial average to employ and how to deform the basic equation. It may be necessary to evaluate whether the modeling well approximates the original system, e.g., by evaluating the similarity of the structure of the solution space, as discussed in the previous paragraph.

We have proposed a model study for thermal convection of miscible fluids, where in reality the width of the transitional layer grows in time and the convection pattern drastically changes when the width reaches a certain value. The model system inherits most of the time-dependent properties of the original system, but discards the growth of the horizontally averaged width of the transitional layer between the miscible fluids. This artificial model system permits us to perform a systematic analysis of the pattern transition of the convection. We expect similar modeling approaches to be useful for understanding non-steady pattern transitions in complex systems.

Appendix A

Proofs of Some Claims

In this chapter, we prove some mathematical claims appearing in Section 3.6.

A.1 Invariance of symmetry of the model system in time development

Theorem A.1.1. *Let $\phi = [\psi, \Theta, \Sigma]^T$ be a convection. If ϕ is invariant under $\mathscr{F}_{\text{vis}}$ at $t = 0$, then it is also invariant for all $t \geq 0$. Similarly, if ϕ is invariant under $\mathscr{F}_{\text{therm}}$ at $t = 0$, then it is also invariant for all $t \geq 0$.*

Proof. Remember the governing equations of the model:

$$\begin{aligned}
\partial_t \nabla^2 \psi + J(\psi, \nabla^2 \psi) &= -RaPr\partial_x(\Theta - B\Sigma) + Pr\nabla^2\nabla^2\psi, \\
\partial_t \Theta + J(\psi, \Theta) + \frac{1}{2}(\partial_x \psi) &= \nabla^2 \Theta, \\
\partial_t \Sigma - (\partial_x \psi)(\partial_z S_\delta) &= \frac{1}{Le}\nabla^2 \Sigma,
\end{aligned}$$

where

$$\begin{aligned}
J(a, b) &= (\partial_z a)(\partial_x b) - (\partial_x a)(\partial_z b), \\
S_\delta(z) &= \frac{1}{2}\text{erfc}\left(\frac{z}{\delta}\right), \\
\text{erfc}(x) &= \frac{2}{\sqrt{\pi}} \int_x^\infty e^{-\xi^2} d\xi.
\end{aligned}$$

First, we shall show that $\mathscr{F}_{\text{vis}}[\phi]$ and $\mathscr{F}_{\text{therm}}[\phi]$ also satisfy the governing equations and the boundary conditions. We denote

$$\begin{bmatrix} \psi_{\text{vis}} \\ \Theta_{\text{vis}} \\ \Sigma_{\text{vis}} \end{bmatrix} = \mathscr{F}_{\text{vis}} \begin{bmatrix} \psi \\ \Theta \\ \Sigma \end{bmatrix}, \quad \text{i.e.,} \quad \begin{cases} \psi_{\text{vis}}(x, z, t) = -\psi(x, -z, t), \\ \Theta_{\text{vis}}(x, z, t) = -\Theta(x, -z, t), \\ \Sigma_{\text{vis}}(x, z, t) = -\Sigma(x, -z, t). \end{cases}$$

By simple computations, we can show that all the terms in the governing equations change those signs when substituting ψ_{vis}, Θ_{vis} and Σ_{vis} into ψ, Θ and Σ. The only coefficient that depends on z is

$$\partial_z S_\delta(z) = -\frac{1}{\sqrt{\pi}\delta} e^{-z^2/\delta^2},$$

which is invariant under $z \mapsto -z$. Thus all coefficients in the governing equations do not change when z is replaced by $-z$. Combining above observations and the governing equations, we can see $[\psi_{\mathrm{vis}}, \Theta_{\mathrm{vis}}, \Sigma_{\mathrm{vis}}]^T$ enjoys the governing equation. Furthermore, these functions satisfy the boundary conditions:

$$\psi_{\mathrm{vis}}(x, \pm 1, t) = \partial_z \psi_{\mathrm{vis}}(x, \pm 1, t) = \Theta_{\mathrm{vis}}(x, \pm 1, t) = \Sigma_{\mathrm{vis}}(x, \pm 1, t) = 0.$$

Similar arguments hold also in the case of $\mathscr{F}_{\mathrm{therm}}[\phi]$.

Here we consider an orbit in the phase space $\phi(t)$ $(t \geq 0)$ that satisfy the governing equations and boundary conditions. Suppose $\phi(0)$ has the symmetry of viscous coupling, i.e., $\mathscr{F}_{\mathrm{vis}}[\phi(0)] = \phi(0)$. If $\phi(t)$ violates the symmetry of viscous coupling for some $t > 0$, then there exist two different orbits $\phi(t)$ and $\mathscr{F}_{\mathrm{vis}}[\phi](t)$ that satisfy the governing equations and boundary conditions. It contradicts with the uniqueness of solution because both of them start from $\phi(0)$ at $t = 0$. Similar arguments hold when the thermal coupling symmetry is supposed at $t = 0$. □

A.2 Orthogonality of thermal and viscous coupling functional spaces

Definition A.2.1. *Let $\mathscr{X}$ be a function space defined by*

$$\mathscr{X} = \left\{ f \colon \mathbb{R}/L_x \times [-1,1] \to \mathbb{C}^3 \;\middle|\; \int_{\mathbb{R}/L_x \times [-1,1]} |f(x,z)|^2 dx dz < \infty \right\},$$

where $L_x > 0$ and $\mathbb{R}/L_x$ is a quotient of $\mathbb{R}$ divided by the equivalence relation $\sim$ defined by $x \sim y \Leftrightarrow x - y \in L_x\mathbb{Z}$. An inner product $\langle \cdot, \cdot \rangle$ on $\mathscr{X}$ is defined by

$$\langle f, g \rangle = \int_{\mathbb{R}/L_x \times [-1,1]} f(x,z) \cdot g(x,z) dx dz, \quad (f, g \in \mathscr{X})$$

where $\cdot$ is the inner product in $\mathbb{C}^3$, i.e., $u \cdot v = \sum_{i=1}^3 \overline{u_i} v_i$ for $u = (u_1, u_2, u_3), v = (v_1, v_2, v_3) \in \mathbb{C}^3$.

We define subspaces $\mathscr{X}_{\mathrm{vis}}, \mathscr{X}_{\mathrm{therm}} \subseteq \mathscr{X}$ by

$$\mathscr{X}_{\mathrm{vis}} = \{ f \in \mathscr{X} \mid f(x,-z) = -f(x,z) \},$$
$$\mathscr{X}_{\mathrm{therm}} = \left\{ f \in \mathscr{X} \;\middle|\; f\left(x + \frac{L_x}{4}, -z\right) = -f(x,z) \right\}.$$

We define $\mathscr{P}_{\mathrm{vis}}\colon \mathscr{X} \to \mathscr{X}$ *and* $\mathscr{P}_{\mathrm{therm}}\colon \mathscr{X} \to \mathscr{X}$ *by*

$$\mathscr{P}_{\mathrm{vis}}[f](x,z) = \frac{1}{2}\left(f(x,z) - f(x,-z)\right),$$

$$\begin{aligned}&\mathscr{P}_{\mathrm{therm}}[f](x,z)\\ &= \frac{1}{4}\left(f(x,z) - f\left(x+\frac{L_x}{4},-z\right) + f\left(x+\frac{2L_x}{4},z\right) - f\left(x+\frac{3L_x}{4},-z\right)\right).\end{aligned}$$

Theorem A.2.2. *$\mathscr{P}_{\mathrm{vis}}$ and $\mathscr{P}_{\mathrm{therm}}$ are commutative orthogonal projections to $\mathscr{X}_{\mathrm{vis}}$ and $\mathscr{X}_{\mathrm{therm}}$, respectively.*

Proof. It is obvious that $\mathscr{P}_{\mathrm{vis}}$ and $\mathscr{P}_{\mathrm{therm}}$ are bounded linear operators.

For any $f \in \mathscr{X}$, it holds that

$$\mathscr{P}_{\mathrm{vis}}[f](x,-z) = \frac{1}{2}\left(f(x,-z) - f(x,z)\right) = -\mathscr{P}_{\mathrm{vis}}[f](x,z)$$

and

$$\begin{aligned}&\mathscr{P}_{\mathrm{therm}}[f]\left(x+\frac{L_x}{4},-z\right)\\ &= \frac{1}{4}\left(f\left(x+\frac{L_z}{4},-z\right) - f\left(x+\frac{2L_x}{4},z\right) + f\left(x+\frac{3L_x}{4},-z\right) - f\left(x,z\right)\right)\\ &= -\mathscr{P}_{\mathrm{therm}}[f](x,z).\end{aligned}$$

Furthermore, $\mathscr{P}_{\mathrm{vis}}[f] = f$ holds for every $f \in \mathscr{X}_{\mathrm{vis}}$, and $\mathscr{P}_{\mathrm{therm}}[g] = g$ holds for every $g \in \mathscr{X}_{\mathrm{therm}}$. Thus $\mathscr{P}_{\mathrm{vis}}\mathscr{X} = \mathscr{X}_{\mathrm{vis}}$ and $\mathscr{P}_{\mathrm{therm}}\mathscr{X} = \mathscr{X}_{\mathrm{therm}}$ hold.

For any $f \in \mathscr{X}$, it holds that

$$\mathscr{P}_{\mathrm{vis}}\left[\mathscr{P}_{\mathrm{vis}}[f]\right](x,z) = \frac{1}{2}\left(\mathscr{P}_{\mathrm{vis}}[f](x,z) - \mathscr{P}_{\mathrm{vis}}[f](x,-z)\right) = \mathscr{P}_{\mathrm{vis}}[f](x,z)$$

and

$$\begin{aligned}&\mathscr{P}_{\mathrm{therm}}\left[\mathscr{P}_{\mathrm{therm}}[f]\right](x,z)\\ &= \frac{1}{4}\left(\mathscr{P}_{\mathrm{therm}}[f](x,z) - \mathscr{P}_{\mathrm{therm}}[f]\left(x+\frac{L_x}{4},-z\right)\right.\\ &\qquad\left. + \mathscr{P}_{\mathrm{therm}}[f]\left(x+\frac{2L_x}{4},z\right) - \mathscr{P}_{\mathrm{therm}}[f]\left(x+\frac{3L_x}{4},-z\right)\right)\\ &= \mathscr{P}_{\mathrm{therm}}[f](x,z).\end{aligned}$$

Thus $\mathscr{P}_{\mathrm{vis}}$ and $\mathscr{P}_{\mathrm{therm}}$ are projections.

For any $f \in \mathscr{X}$,

$$\begin{aligned}
&\mathscr{P}_{\text{vis}}[\mathscr{P}_{\text{therm}}[f]](x,z) \\
&= \frac{1}{2}\left(\mathscr{P}_{\text{therm}}[f](x,z) - \mathscr{P}_{\text{therm}}[f](x,-z)\right) \\
&= \frac{1}{8}\left(f(x,z) - f\left(x+\frac{L_x}{4},-z\right) + f\left(x+\frac{2L_x}{4},z\right) - f\left(x+\frac{3L_x}{4},-z\right)\right. \\
&\qquad \left. -f(x,-z) + f\left(x+\frac{L_x}{4},z\right) - f\left(x+\frac{2L_x}{4},-z\right) + f\left(x+\frac{3L_x}{4},z\right)\right) \\
&= \frac{1}{4}\left(\mathscr{P}_{\text{vis}}[f](x,z) - \mathscr{P}_{\text{vis}}[f]\left(x+\frac{L_x}{4},-z\right)\right. \\
&\qquad \left. +\mathscr{P}_{\text{vis}}[f]\left(x+\frac{2L_x}{4},z\right) - \mathscr{P}_{\text{vis}}[f]\left(x+\frac{3L_x}{4},-z\right)\right) \\
&= \mathscr{P}_{\text{vis}}[\mathscr{P}_{\text{therm}}[f]](x,z).
\end{aligned}$$

Thus $\mathscr{P}_{\text{vis}}$ and $\mathscr{P}_{\text{therm}}$ are commutative.

Finally, we shall show $\mathscr{P}_{\text{vis}}$ and $\mathscr{P}_{\text{therm}}$ are orthogonal projections. It is sufficient to prove that

$$\langle \mathscr{P}_{\text{vis}}[f], g\rangle = \langle f, \mathscr{P}_{\text{vis}}[g]\rangle \tag{A.1}$$

and

$$\langle \mathscr{P}_{\text{therm}}[f], g\rangle = \langle f, \mathscr{P}_{\text{therm}}[g]\rangle \tag{A.2}$$

for any $f, g \in \mathscr{X}$. We can see easily

$$\langle f(x,-z), g(x,z)\rangle = \langle f(x,z), g(x,-z)\rangle$$

for any $f, g \in \mathscr{X}$. It proves the identity (A.1). Furthermore, by simple computations, we have the following properties for any $f, g \in \mathscr{X}$:

$$\begin{aligned}
\left\langle f(x,z), g\left(x+\frac{L_x}{2},z\right)\right\rangle &= \left\langle f\left(x+\frac{L_x}{2},z\right), g\left(x+L_x,z\right)\right\rangle \\
&= \left\langle f\left(x+\frac{L_x}{2},z\right), g\left(x,z\right)\right\rangle, \\
\left\langle f\left(x,z\right), g\left(x+\frac{L_x}{4},z\right)\right\rangle &= \left\langle f\left(x+\frac{3L_x}{4},z\right), g\left(x+L_x,z\right)\right\rangle \\
&= \left\langle f\left(x+\frac{3L_x}{4},z\right), g\left(x,z\right)\right\rangle, \\
\left\langle f\left(x,z\right), g\left(x+\frac{3L_x}{4},z\right)\right\rangle &= \left\langle f\left(x+\frac{L_x}{4},z\right), g\left(x+L_x,z\right)\right\rangle \\
&= \left\langle f\left(x+\frac{L_x}{4},z\right), g\left(x,z\right)\right\rangle.
\end{aligned}$$

Then the identity (A.2) follows immediately. □

Theorem A.2.3. *Let V be a metric space with an inner product $\langle \cdot, \cdot \rangle_V : V \times V \to \mathbb{R}$. Let $P, Q : V \to V$ be commutative orthogonal projections. Then*

$$W_P \perp W_Q$$

holds, where W_P and W_Q are subspaces of V satisfying the orthogonal direct sum decompositions

$$PV = W_P \oplus (PV \cap QV), \quad QV = W_Q \oplus (PV \cap QV).$$

Proof. First, we prove that $PQV = PV \cap QV$. If $u \in PQV = QPV$, obviously $u \in PV$ and $v \in QV$, thus $PQV \subseteq PV \cap QV$ holds. If $u \in PV \cap QV$, then $u = Pv = Qw$ for some $v, w \in V$. Since P and Q are projections, it follows that

$$PQu = PQQw = PQw = Pu = PPv = Pv = u \in PQV.$$

Thus $PV \cap QV \subseteq PQV$. Therefore $PQV = PV \cap QV$.

Since P and Q are orthogonal projections, we have orthogonal direct sum decompositions

$$PV = W_P \oplus QPV, \quad QV = W_Q \oplus PQV,$$

where $W_P = PV \cap \mathrm{Ker}\, Q$ and $W_Q = QV \cap \mathrm{Ker}\, P$. Take arbitrary $u \in W_P$ and $v \in W_Q$. There exists $u_0 \in W_P$ such that $u = Pu_0$ since $W_P \subseteq PV$. Then

$$\langle u, v \rangle_V = \langle Pu_0, v \rangle_V = \langle u_0, Pv \rangle_V = \langle u_0, 0 \rangle_V = 0.$$

Therefore $W_P \perp W_Q$. □

From Theorem A.2.2 and A.2.3, the following is deduced.

Theorem A.2.4. *Consider orthogonal direct sum decompositions*

$$\mathscr{X}_{\mathrm{vis}} = \hat{\mathscr{X}}_{\mathrm{vis}} \oplus (\mathscr{X}_{\mathrm{vis}} \cap \mathscr{X}_{\mathrm{therm}}), \quad \mathscr{X}_{\mathrm{therm}} = \hat{\mathscr{X}}_{\mathrm{therm}} \oplus (\mathscr{X}_{\mathrm{vis}} \cap \mathscr{X}_{\mathrm{therm}}).$$

Then $\hat{\mathscr{X}}_{\mathrm{vis}} \perp \hat{\mathscr{X}}_{\mathrm{therm}}$ holds.

Acknowledgments

I would like to express my deep gratitude to Prof. Michio Yamada. He gave me tremendous knowledge and ways of thinking about physical and mathematical sciences, especially chaos and turbulence theory. He guided me kindly and patiently through fruitful discussions in and out of seminars.

I also would like to express my sincere appreciation to Prof. Shin-ichi Takehiro. He provided me with not only expertise in physics and geophysics but also techniques of numerical analyses. His simple and essential advice based on his insights and experiences has genuinely enriched my research.

Without their incredible support and heartful encouragement, I could not reach any results in this thesis. I repeatedly express my most profound appreciation to both professors.

Prof. Sato and Prof. Ishimoto gave me fruitful advice on my study. Prof. Obuse, Prof. Eiichi Sasaki, Prof. Inubushi, Dr. Kimura, Prof. Yohei Sasaki, and Mr. Hirofumi Sasaki provided me with valuable comments. I also had meaningful discussions with Prof. Misuzhima, Prof. Toh, Prof. Matsumoto, Dr. Hiruta, and Dr. Kishi.

I also would like to thank my colleagues at Kyoto University, especially at Research Institute for Mathematical Sciences. Conversations and discussions with them encouraged me to keep on studying.

This work was partially supported by the Japan Society for the Promotion of Science, KAKENHI Grants Nos. 15K13458, 15H05834, 17H02860, 19H01947, and 21H01155. This work was also supported by the Research Institute for Mathematical Sciences, a Joint Usage/Research Center located in Kyoto University. The numerical calculations were performed on the computer systems of the Research Institute for Mathematical Sciences, Kyoto University.

The ISPACK library for spectral transform (http://www.gfd-dennou.org/arch/ispack), and its Fortran90 wrapper library, SPMODEL [23] were used. The products of the Dennou Ruby project (http://www.gfd-dennou.org/library/ruby) and gnuplot were used for visualization.

Finally, I would like to express my genuine gratitude to my family. My parents raised me with deep affection and let me pursue my curiosity by supporting me financially and mentally. My wife always gave me vitality for study and peace of mind. I am proud of my family from the bottom of my heart.

References

[1] Chandrasekhar, S.: Hydrodynamic and hydromagnetic stability. Courier Corporation (2013).

[2] Colinet, P., Legros, J. C.: On the Hopf bifurcation occurring in the two-layer Rayleigh-Bénard convective instability. Physics of fluids 6.8, 2631-2639, (1994)

[3] Cserepes, L., Rabinowicz. M.: Gravity and convection in a two-layer mantle. Earth and Planetary Science Letters 76.1-2,193-207 (1985)

[4] Cserepes, L., Rabinowicz, M., Rosemberg-Borot, C.: Three-dimensional infinite Prandtl number convection in one and two layers with implications for the Earth's gravity field. Journal of Geophysical Research: Solid Earth 93.B10,12009-12025 (1988)

[5] Davaille, A.: Two-layer thermal convection in miscible viscous fluids. Journal of Fluid Mechanics 379, 223-253 (1999)

[6] Degen, M. M., Colovas, P. W., David A. C.: Time-dependent patterns in the two-layer Rayleigh-Bénard system. Physical Review E 57.6, 6647(1998):

[7] Diwakar, S. V., *et al.*: Stability and resonant wave interactions of confined two-layer Rayleigh-Bénard systems. Journal of Fluid Mechanics 754, 415-455 (2014)

[8] Fujimura, K., Renardy, Y. Y.: The 2:1 steady/Hopf mode interaction in the two-layer Bénard problem. Physica D: Nonlinear Phenomena 85.1-2,25-65 (1995)

[9] Ishikawa, T., Takehiro, S., and Yamada, M.: Model system for the transient behavior of double diffusive convection in two miscible layers. Japan Journal of Industrial and Applied Mathematics (2022): 1-25.

[10] Kawahara, Genta, and Shigeo Kida.: Periodic motion embedded in plane Couette turbulence: regeneration cycle and burst. Journal of Fluid Mechanics 449, 291-300 (2001)

[11] Le Bars, M., Davaille, A.: Stability of thermal convection in two superimposed miscible viscous fluids. Journal of Fluid Mechanics, **471**, 339-363 (2002)

[12] Liu, Qiu-Sheng, *et al.*: Oscillatory instabilities of two-layer Rayleigh-Marangoni-Benard convection. Acta Astronautica 59.1-5,40-45 (2006)

[13] Mizushima, J.: Oscillatory Instability in Two-layer Fluid Contained in a Rectangular Cavity and Its Driving Mechanism. Journal of the Physical Society of Japan 87.8,084401 (2018)

[14] Nepomnyashchy, A. A., Simanovskii. I. B.: Influence of thermocapillary effect and interfacial heat release on convective oscillations in a two-layer system. Physics of Fluids 16.4,1127-1139 (2004)

[15] Prakash, A. T., Koster. J. N.: Convection in multiple layers of immiscible liquids in a shallow cavity-I. Steady natural convection. International journal of multiphase flow 20.2,383-396 (1994)

[16] Rasenat, S., Busse, F. H., Rehberg, I.: A theoretical and experimental study of double-layer convection." Journal of Fluid Mechanics 199, 519-540 (1989)

[17] Renardy, Y., Joseph. D. D.: Oscillatory instability in a Bénard problem of two fluids. The Physics of fluids 28.3, 788-793 (1985)

[18] Renardy, Y. Y.: Pattern formation for oscillatory bulk-mode competition in a two-layer Bénard problem. Zeitschrift für angewandte Mathematik und Physik ZAMP 47.4, 567-590 (1996):

[19] Richter, F. M., Johnson, C. E.: Stability of a chemically layered mantle. Journal of Geophysical Research 79.11, 1635-1639 (1974)

[20] Simanovskii, I. B., Nepomnyashchy, A. A.: Nonlinear development of oscillatory instability in a two-layer system under the combined action of buoyancy and thermocapillary effect. Journal of Fluid Mechanics 555, 177-202 (2006):

[21] Simanovskii, I. B.: The influence of the interfacial heat release on nonlinear convective oscillations in two-layer systems. Physics of Fluids 25.7, 072106 (2013)

[22] Turner, J. S.: Buoyancy effects in fluids. Cambridge University Press (1973)

[23] Takehiro, S., Odaka, M., Ishioka, K., Hayashi, Y.-Y.: SPMODEL: A series of Hierarchical Spectral Models for Geophysical Fluid Dynamics, Nagare Multimedia. http://www.nagare.or.jp/mm/2006/spmodel (2006) Accessed 19 February 2022.

[24] Wilczynski, F., Hughes, D. W.: Stability of two-layer miscible convection. Physical Review Fluids 4.10, 103502 (2019)

[25] Yanagisawa, T., Kurita, K,: A process of mixing in a two-layered thermal convection system (Mathematical Aspects of Thermal Convection Dynamics : Structure of Flow Fields). (Japanese) RIMS Kokyuroku 1115, 181-194 (1999):